Beam finite element models with node dependent kinematics and arbitrary displacement fields over the cross-section

Beam Finite Element models with Node Dependent Kinematics and Arbitrary Displacement Fields over the Cross-Section

E. Carrera[a,b,*], D. Scano[a,†]

[a]MUL^2 Lab, Department of Mechanical and Aerospace Engineering, Politecnico di Torino, Corso Duca degli Abruzzi 24, 10129 Torino, Italy

[b]Department of Mechanical Engineering, College of Engineering, Prince Mohammad Bin Fahd University P.O. Box 1664. Al Khobar 31952. Kingdom of Saudi Arabia

Submitted to
Mechanics of Advanced Materials and Structures

Author for correspondence:
Daniele Scano
MUL^2 Lab, Department of Mechanical and Aerospace Engineering,
Politecnico di Torino,
Corso Duca degli Abruzzi 24,
10129 Torino, Italy,
tel: +39 011 090 4390,
e-mail: daniele.scano@polito.it

*Professor of Aeronautics and Astronautics. E-mail: erasmo.carrera@polito.it
†PhD Student. E-mail: daniele.scano@polito.it

Abstract: *The present paper proposes new, improved one-dimensional finite elements that use the node-dependent kinematics method, i.e., each node may adopt a different expansion over the cross-section without using a special coupling method. Furthermore, the presented method is able to choose independent models for each of the three displacement variables. In particular, Taylor-based and Lagrange-based functions have been chosen as expansions for the cross-sections. These two outcomes are possible through the use of the Carrera Unified Formulation, which subdivides the three-dimensional displacement field into a cross-section domain and an axis domain. Starting from the principle of virtual displacements, the governing equations and finite element matrices are obtained. In numerical results, compact and thin-walled beams have been studied and subjected to various loading conditions, including bending and torsion-bending. The selected cases are compared with existing literature or with high-refined CUF-based solutions. The accuracy of the models presented is assessed for both displacements and stress components. The results show that the choice of the 'best' computational models in terms of accuracy vs degree of freedom is problem-dependent. Finally, the Node-dependent kinematics method permits the selection of the most suitable expansions for each cross-section.*

Keywords: Finite element method; beam models; Carrera Unified Formulation; Taylor polynomials; Lagrange polynomials; Node-dependent Kinematics.

1 Introduction

The section-wise deformation of beams. The use of one-dimensional (1D) models persists nowadays in engineering design despite the introduction of more computational expansive three-dimensional (3D) theories. The 1D models, also commonly denoted as beam models, are adopted in several branches of engineering, i.e., civil, biomedical, and aerospace fields. To name a few, reinforced concrete beams, helicopter rotor blades, and aircraft wings may be studied to reach useful results.

The use of one-dimensional (1D) models persists nowadays in engineering design despite the introduction of more computational expansive three-dimensional (3D) theories. The 1D models, also commonly denoted as beam models, are adopted in several branches of engineering, i.e., civil, biomedical, and aerospace fields. To name a few, reinforced concrete beams, helicopter rotor blades, and aircraft wings may be studied to reach useful results. The deformation

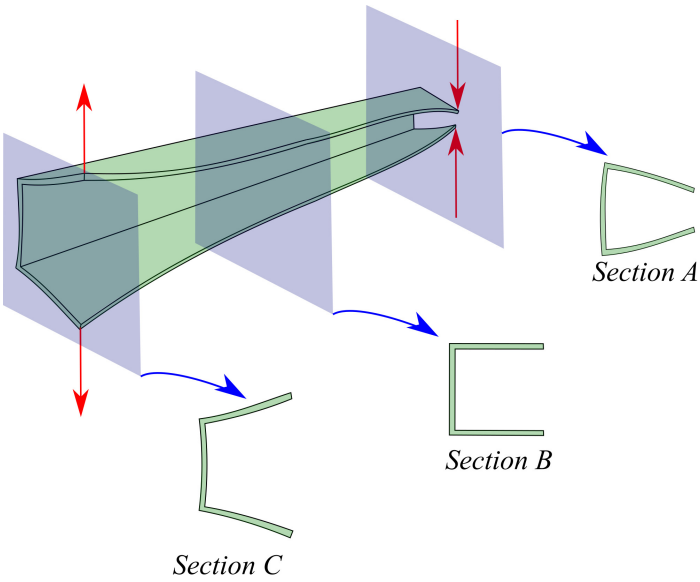

Figure 1: Localized deformations on different sections of a beam structure.

and the state of stresses in a structure are affected by several parameters. Typically, they are identified by the kind of loading, boundary conditions, materials, and properties of the geometry, even though other specific parameters may influence the equilibrium state, see Carrera and Zappino for more information [1]. In Fig. 1, a beam with a C cross-section is shown. The structure is loaded by forces at the tips, while the mid-span section is clamped. Each of the three considered sections undergoes different deformations. In particular, the deformed state of equilibrium is a "section-wise" property of the beam. In this example, Sections C and A are subjected to a significant deformation of the thin-walled structure, whereas Section B is kept fixed. Thus, it is evident that each section should be conveniently approximated by different refined beam theories.

Classical and Refined beam approaches. The review of beam models begins with the classical theories. The Euler-Bernoulli beam model [2] is commonly used to accurately evaluate dis-

placements in isotropic slender structures, though it does not account for transverse shear effects. In contrast, the Timoshenko beam model [3] can capture constant shear effects. Commercial Finite Element (FE) programs typically utilize beam elements with six degrees of freedom (DOF) per node, consisting of three displacements and three rotations. For further details, see Bathe's work [4].

Since the classical beam elements are affected by some limitations, such as the limitation in describing local effects and non-linear deformations, researchers have developed more effective 3D elements. In these elements, only three displacements are used for each Finite Element (FE) node. Interested readers can refer to Argyris [5]. However, the use of these models is constrained by the high computational cost. Furthermore, it is common to study thin-walled structures (similar to the one depicted in Fig. 1) by adopting two-dimensional plate/shell elements. Usually, they have five and six DOFs for each node [6].

Several refined beam models have been proposed to address the limitations of classical beam theories. First, axiomatic theories are briefly reviewed, where scientists made 'a priori' or intuitive assumptions about the deformed states of loaded structures, as discussed in Novozhilov's influential work [7]. Comprehensive reviews of advanced beam models are available in the studies by Kapania and Raciti [8, 9], as well as Carrera *et al.* [10]. Washizu highlighted the importance of the use of higher-order models in his relevant book [11]. Furthermore, Vlasov [12] introduced the use of warping functions to account for cross-section deformation, enabling the analysis of thin-walled structures. This method has been employed by Friberg [13], Ambrosini *et al.* [14], and Mechab *et al.* [15]. Another approach, known as Generalized Beam Theory (GBT), was proposed by Schardt [16]. GBT improves classical theories by using piece-wise beam descriptions of thin-wall sections, which permit the capture of complex phenomena like warping and distortional effects. Ganapathi *et al.* [17] developed a three-node beam FE that includes transverse shear and warping torsion. This approach addresses shear deformation using a higher-order cosine function. Levinson [18] proposed a new beam theory that incorporates cross-section warping while respecting shear-free conditions on the lateral surfaces. Kant and Manjunath [19] introduced higher-order displacement models using the C^0 FE method to analyse laminated composite beams. They varied the displacement component along the axis direction from first to fourth order while keeping the displacement component in the thickness direction constant, similar to classical models. Further refinements were proposed by the same authors in [20] and [21], where they assumed higher-order terms for the transverse displacement.

The Carrera Unified Formulation. The Carrera Unified Formulation (CUF) was initially proposed by Carrera [22, 23] for plates and shells and later extended to beam formulations by Carrera and Giunta [24]. Within the CUF framework, cross-sectional kinematics can be approximated using any type of function. Carrera *et al.* [25] applied Taylor-like expansions up to the fourth order to analyze compact and thin-walled airfoil sections. Additionally, Carrera *et al.* [26] demonstrated the advantages of higher-order theories in the study of shell-like structures. Carrera and Petrolo [27] introduced three-, four-, and nine-node Lagrange-like

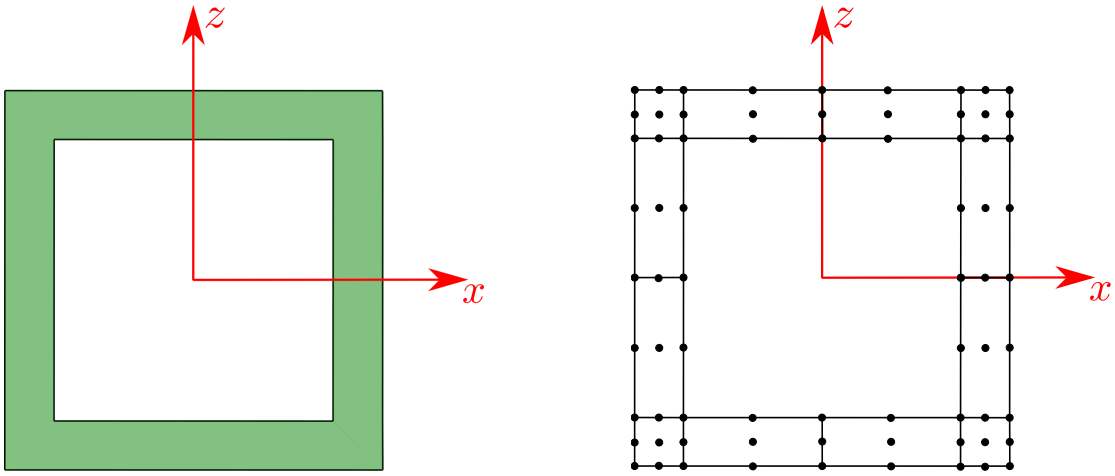

(a) Geometry (b) Lagrange expansions

Figure 2: Use of the Lagrange expansions for the study of an hollow square cross-section.

expansions to investigate composite beams. For example, Fig. 2 illustrates a hollow square cross-section, showing that these elements allow for a highly accurate cross-sectional discretization comparable to a 3D model. The mathematical details are provided in Section 2.2. Moreover, Pagani *et al.* [28] employed sixteen-node Lagrange expansions for composite structures.

Global-local models. The above-discussed papers assumed the same structural model for each section of the beam. In modern engineering, however, the development of highly deformable structures needs very refined results. Since this leads to an incredible rise in computational time, researchers have proposed several methods to use more refined models only in some parts of the structures to study higher-order effects, see Reddy [29]. In this context, assuring the compatibility of the displacements between different models is a difficult task. In the last decades, several approaches have been proposed. In the following, a review of some interesting methods is reported. See the work of Noor [30] for more details.

For example, Fish *et al.* [31] developed a multi-grid method for exchanging information between coarse and fine meshes using an iterative algorithm. One of the most widely adopted techniques is the use of Lagrange multipliers, as discussed by Prager [32]. In this context, Park and Felippa [33] proposed a continuum-based variational principle for deriving discrete governing equations for partitioned structural systems. Carrera *et al.* [34] applied this approach within the beam formulation of the CUF, combining Taylor expansions of varying polynomial orders. Additionally, Aminpour *et al.* [35] and Ransom [36] utilized a spline method to couple domains with different meshes, while Brezzi and Marini [37] proposed a similar approach within the three-field formulation. Blanco *et al.* [38, 39] introduced an eXtended Variational Formulation (XVF), which couples different kinematic models using the Lagrange multiplier method. Compatibility between two zones can be enforced through the use of an overlapping region. Specifically, Ben Dhia and co-workers [40, 41] proposed the Arlequin method with Lagrange multipliers. This approach was later applied to beam

models within the framework of CUF by Biscani *et al.* [42]. Researchers have also explored linking 1D and 3D domains to reduce computational costs and improve efficiency [43]. In Klarmann *et al.* [44], the cross-sectional deformation is handled by the solid part, while beam elements capture only the constant rotation of the cross-section. Hartloper *et al.* [45] studied thin-walled structures using a coupling method that incorporates the effects of cross-sectional warping. Zappino and Carrera *et al.* [46] addressed the behavior of complex geometries by employing the CUF, integrating beam, shell, and solid models. Finally, Carrera and coworkers have also developed a two-step global/local technique [47, 48]. In the first step, a global analysis is conducted using a commercial code (e.g., ABAQUS or Femap/NX Nastran). Then, a more refined analysis is performed with a CUF-generated model for a localised part of the structure.

Aim of the present paper. The principal goal of this work is to create an FE approach where

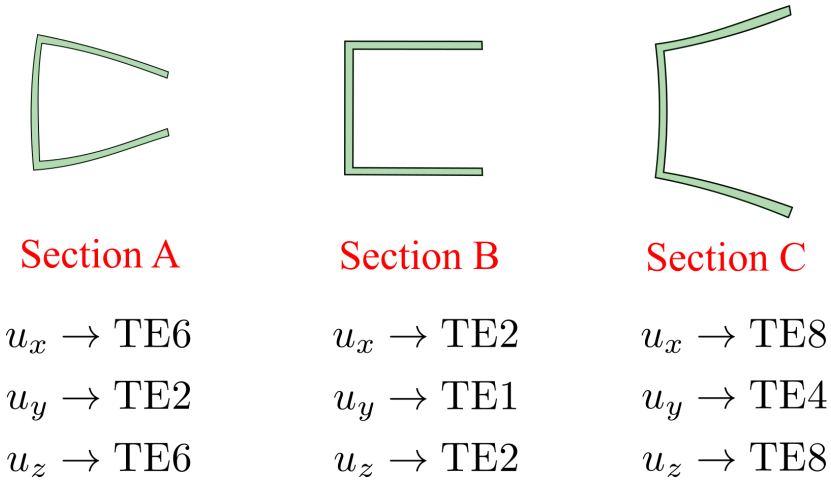

Figure 3: Use of different models for the study of the three sections of Fig. 1.

there is the possibility to choose in a completely independent manner in order to tailor the accuracy and the computational cost. It is useful to use the example shown in Fig. 1 to explain this concept more precisely. Figure 3 illustrates the three cross-sections. In this case, it is possible to choose the theory for each displacement variable as well as changing the expansions for each cross-section. In this particular example, more refined cases are required in the external sections. In Section 5.3, a similar example is deeply studied by adopting both Taylor and Lagrange expansions.

The first step is to employ a method that allows for independent displacement variables in a unified and straightforward manner. In past literature, scholars have often proposed ad-hoc theories tailored to predict specific structural behaviours accurately. Consequently, for each new problem, researchers had to redefine a theory and recalculate the governing equations. Frameworks such as GBT and the CUF aim to create a unified approach for structural analysis, enabling the use of various models without altering the fundamental mathematical assumptions. To address these challenges, Carrera *et al.* [49] proposed a new beam approach based on the mathematical principles of the CUF, allowing for the creation of refined models

within the same framework. This eliminates the need to rewrite governing equations each time the displacement field changes. However, in the 'classical' CUF, displacement variables are studied using the same expansion function, which limits the flexibility to create tailored theories and control computational costs. To overcome this, the unified formulation has been redefined to facilitate the development of specialized beam theories within the finite element method. A scalar function (FN) is used as the basis for constructing the global stiffness matrix, avoiding the penalization techniques that exclude terms, as described in [50]. This approach ensures the stiffness matrix has consistent dimensions, meaning its size—along with the unknown and load vectors—depends on the chosen kinematic model. The full details of this method are provided in the foundational work by Carrera *et al.* [49].

The second step is the possibility of having a section-wise description. Carrera and co-workers have implemented an approach called Node-Dependent Kinematics (NDK). As the name implies, it is possible to choose a different model for each FE node without using other mathematical equations. Using the FEM, there are no issues in joining different structural theories. This approach was first proposed by Carrera and Zappino [1] for linear static analysis. Lagrange-like and Taylor-like expansions are adopted over the cross-section. Li *et al.* [51] used Legendre and Taylor expansions adopted in the same FE models. Zappino *et al.* [52] extended the use of these expansions also to thin-walled structures. Carrera *et al.* [53] used this method in shell formulation. In the previous papers, in the single FE node, the three displacement variables were the same, not allowing models similar to those seen in Fig. 3. On the contrary, this work presents a new method that connects the possibility of using different expansions for each displacement variable and the capabilities of the NDK.

Structure of the work. This paper is organized as follows: (a) Section 2 provides an overview of the models and explains how Taylor- and Lagrange-based expansions are combined to develop new theories. (b) Section 3 discusses the principles of the Unified Formulation, its integration with the finite element method, and the mathematical details of the Node-dependent Kinematics approach. (c) Section 4 derives the governing equations using the principle of virtual displacements. (d) Section 4.2 illustrates the assembly of the stiffness matrix and load vector within the Unified Formulation using a simple example. (e) Section 5 presents the results for displacements and stresses. (f) Lastly, Section 6 summarizes the key findings.

2 Proposed Beam finite element

Consider the thin-walled beam depicted in Fig. 4. A Cartesian reference system is adopted. The cross-section, A, lies in the x-z plane. The cross-section may be divided into the different mathematical domains, denoted as k. The beam axis is aligned with the direction of y. The three-dimensional displacement field is described by the following vector:

$$\mathbf{u}^k(x,y,z) = \left\{ \begin{array}{ccc} u_x^k(x,y,z), & u_y^k(x,y,z), & u_z^k(x,y,z) \end{array} \right\}^T \tag{1}$$

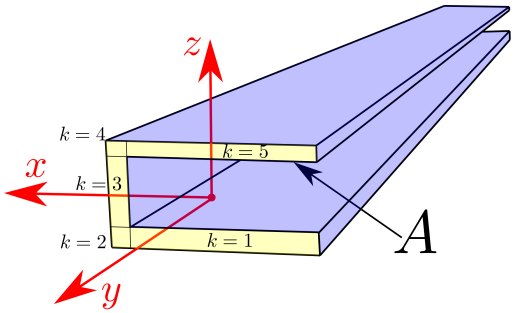

Figure 4: Reference system for a generic beam-like structure.

It is worth noting that u_x^k, u_y^k, and u_z^k can be explicitly written with different theories. This section is devoted to the mathematical details of advanced models which are used in the present work.

2.1 Taylor-based Higher-order theories

Taylor polynomials, specifically 2D polynomials of the form $x^a z^b$, are employed to formulate general Higher-Order Theories (HOTs) for describing the behavior of beam cross-sections. These polynomials use positive integers for both a and b. Within the context of the CUF, Carrera and Giunta [24] initially investigated beams from the first to the fourth orders to account for higher-order effects. When adopting first-order models, Poisson locking is mitigated through the appropriate reduction of material stiffness coefficients.

Uniform theories In the literature concerning the CUF for the beam formulations, a uniform expansion is assumed for all three displacement variables. These models are referred to as *uniform theories*. For instance, a second-order theory can be expressed as follows:

$$\begin{aligned} u_x &= u_{x_1} + xu_{x_2} + zu_{x_3} + x^2u_{x_4} + xzu_{x_5} + z^2u_{x_6} \\ u_y &= u_{y_1} + xu_{y_2} + zu_{y_3} + x^2u_{y_4} + xzu_{y_5} + z^2u_{y_6} \\ u_z &= u_{z_1} + xu_{z_2} + zu_{z_3} + x^2u_{z_4} + xzu_{z_5} + z^2u_{z_6} \end{aligned} \tag{2}$$

Different theories Previous uniform theories presented identical expansions for all three variables. However, this paper also presents results where u_x, u_y, and u_z are approximated by different polynomial orders. For example, the following structural theory is described by a first-order expansion for u_x and u_z, while a second-order expansion is adopted for u_y:

$$\begin{aligned} u_x &= u_{x_1} + xu_{x_2} + zu_{x_3} \\ u_y &= u_{y_1} + xu_{y_2} + zu_{y_3} + x^2u_{y_4} + xzu_{y_5} + z^2u_{y_6} \\ u_z &= u_{z_1} + xu_{z_2} + zu_{z_3} \end{aligned} \tag{3}$$

Thus, this theory is composed of twelve terms, in contrast to the uniform second-order theory (Eq. (2)), which contains eighteen expansion functions.

2.2 Lagrange-based Higher-order theories

The cross-section is approximated with a pattern of Lagrange Points (LPs), which are divided into opportune Lagrange polynomials. The 3D displacement field is, then, a result of an interpolation of the displacements calculated at the LPs. The degree of the interpolation is defined by the number of the employed LPs. For 1D structures, 4 LPs (L4) ensure a bilinear interpolation, a 9 LPs (L9) a quadratic interpolation, and a 16 LPs (L16) a cubic interpolation. The number of DOFs equals the sum of the displacements for each LP. For instance, if a quadratic interpolation is employed, the interpolation functions for the 1D are:

$$\begin{aligned} F_\tau &= \frac{1}{4}(r^2 + rr_\tau)(s^2 + ss_\tau) && \tau = 1,3,5,7 \\ F_\tau &= \frac{1}{2}s_\tau^2(s^2 - ss_\tau)(1-r^2) + \frac{1}{2}r_\tau^2(r^2 - rr_\tau)(1-s^2) && \tau = 2,4,6,8 \\ F_\tau &= (1-r^2)(1-s^2) && \tau = 9 \end{aligned} \tag{4}$$

where r and s vary from -1 to $+1$, whereas r_τ and s_τ are the coordinates of the LPs located in the natural coordinate, see [54] for more details. Thus, the displacement model based on the interpolations functions given in Eq. (4) may be written as follows:

$$\begin{aligned} u_x^k &= F_{u_x1}^k u_{x_1}^k + F_{u_x2}^k u_{x_2}^k + F_{u_x3}^k u_{x_3}^k + F_{u_x4}^k u_{x_4}^k + F_{u_x5}^k u_{x_5}^k + F_{u_x6}^k u_{x_6}^k \\ &\quad + F_{u_x7}^k u_{x_7}^k + F_{u_x8}^k u_{x_8}^k + F_{u_x9}^k u_{x_9}^k \\ u_y^k &= F_{u_y1}^k u_{y_1}^k + F_{u_y2}^k u_{y_2}^k + F_{u_y3}^k u_{y_3}^k + F_{u_y4}^k u_{y_4}^k + F_{u_y5}^k u_{y_5}^k + F_{u_y6}^k u_{y_6}^k \\ &\quad + F_{u_y7}^k u_{y_7}^k + F_{u_y8}^k u_{y_8}^k + F_{u_y9}^k u_{y_9}^k \\ u_z^k &= F_{u_z1}^k u_{z_1}^k + F_{u_z2}^k u_{z_2}^k + F_{u_z3}^k u_{z_3}^k + F_{u_z4}^k u_{z_4}^k + F_{u_z5}^k u_{z_5}^k + F_{u_z6}^k u_{z_6}^k \\ &\quad + F_{u_z7}^k u_{z_7}^k + F_{u_z8}^k u_{z_8}^k + F_{u_z9}^k u_{z_9}^k \end{aligned} \tag{5}$$

2.3 Mixed Taylor-Lagrange Higher-order theories

It would be advantageous to utilize mixed TE-LE (Taylor Expansions-Lagrange Expansions) models to approximate the 3D displacement field. In this approach, display components employ Lagrange or Taylor expansions. For instance, the following model could be proposed:

$$\begin{aligned} u_x^k &= F_{u_x1}^k u_{x_1}^k + F_{u_x2}^k u_{x_2}^k + F_{u_x3}^k u_{x_3}^k + F_{u_x4}^k u_{x_4}^k + F_{u_x5} u_{x_5} + F_{u_x6} u_{x_6} \\ &\quad + F_{u_x7} u_{x_7} + F_{u_x8} u_{x_8} + F_{u_x9} u_{x_9} \\ u_y &= u_{y_1} + x u_{y_2} + z u_{y_3} + x^2 u_{y_4} + xz u_{y_5} + z^2 u_{y_6} \\ u_z &= u_{z_1} + x u_{z_2} + z u_{z_3} + x^2 u_{z_4} + xz u_{z_5} + z^2 u_{z_6} \end{aligned} \tag{6}$$

It is important to note that the actual number of terms for the in-plane displacement, u_x^k, relies on the number of layers. Conversely, the 'TE' terms remain fixed at six. However, it would be possible to adopt reduced models as well.

3 Node-dependent kinematics one-dimensional models

3.1 Unified formulation for beam

In Sections 1 and 2, many literature models have been presented. It would be interesting to have a framework where every model may be used without the necessity to derive the governing equations each time. To this end, the Carrera Unified Formulation (CUF) has the special capability to describe all these models in a compact manner.
In the CUF framework, the 3D field is represented as a general expansion of the displacement variables:

$$\begin{aligned} u_x^k &= F_{u_x\tau}^k(x,z)u_{x_\tau}^k(y) \quad \text{with} \quad \tau = 1,\dots,M_{u_x} \\ u_y^k &= F_{u_y\tau}^k(x,z)u_{y_\tau}^k(y) \quad \text{with} \quad \tau = 1,\dots,M_{u_y} \quad . \\ u_z^k &= F_{u_z\tau}^k(x,z)u_{z_\tau}^k(y) \quad \text{with} \quad \tau = 1,\dots,M_{u_z} \end{aligned} \tag{7}$$

where $F_{u_x\tau}$, $F_{u_y\tau}$, and $F_{u_z\tau}$ represent the expansion functions for the generalized displacements u_{x_τ}, u_{y_τ}, and u_{z_τ}, respectively. The symbol τ represents summation, and M_{u_x}, M_{u_y}, and M_{u_z} indicate the number of expansions for each displacement variable.
On the other hand, the Finite Element Method (FEM) is adopted to discretize the unknowns along the beam axis:

$$\begin{aligned} u_x^k &= N_i(y)F_{u_x\tau}^k(x,z)q_{x_{\tau i}}^k \quad \text{with} \quad \tau = 1,\dots,M_{u_x} \quad \text{and} \quad i = 1,\dots,N_n \\ u_y^k &= N_i(y)F_{u_y\tau}^k(x,z)q_{y_{\tau i}}^k \quad \text{with} \quad \tau = 1,\dots,M_{u_y} \quad \text{and} \quad i = 1,\dots,N_n. \\ u_z^k &= N_i(y)F_{u_z\tau}^k(x,z)q_{z_{\tau i}}^k \quad \text{with} \quad \tau = 1,\dots,M_{u_z} \quad \text{and} \quad i = 1,\dots,N_n \end{aligned} \tag{8}$$

where N_i stand for the shape functions. The repeated subscripts i indicate summation, whereas N_n is the number of the shape functions per element. For the numerical assessments in this study, the classical four-node Lagrange (B4) element is employed. Additional information can be found in Bathe [4].

3.2 Node-dependent kinematics

In the preceding Sections, the expansion functions for the cross-section were equal along all the beam axes. However, it could be useful to adopt different models for different parts of the beam. The Node-dependent kinematics solves this problem by permitting each FE node to have its own structural theories. Figure 5 summarizes this concept graphically, where a B4 finite element with a compact cross-section is shown. The section may be studied by different expansions. For instance, the first node uses two Lagrangian elements for all the displacement variables, whereas the second node uses both Lagrange and Taylor expansions. In the third and fourth nodes, only one LE9 is adopted. Finally, the fourth node uses a first-order expansion for u_x and u_z.
This concept can be summarized mathematically in the followings for the three displacements

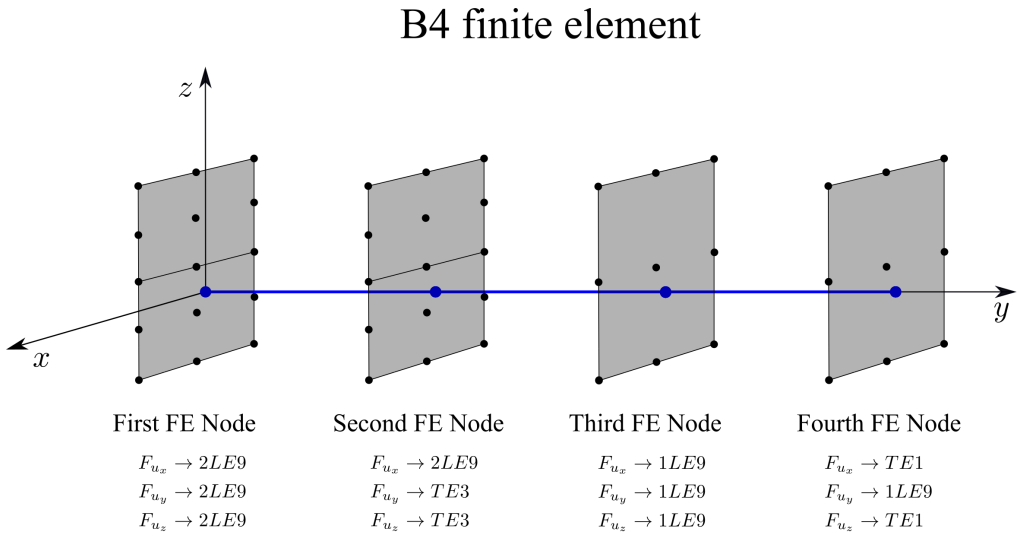

Figure 5: Example of a four-node beam element with the node-dependent kinematics.

variables:

$$\begin{aligned} u_x^k &= N_i(y) F_{u_x\tau}^{ki}(x,z) q_{x_{\tau i}}^k \quad \text{with} \quad \tau = 1,\dots,M_{u_x} \quad \text{and} \quad i = 1,\dots,N_n \\ u_y^k &= N_i(y) F_{u_y\tau}^{ki}(x,z) q_{y_{\tau i}}^k \quad \text{with} \quad \tau = 1,\dots,M_{u_y} \quad \text{and} \quad i = 1,\dots,N_n. \\ u_z^k &= N_i(y) F_{u_z\tau}^{ki}(x,z) q_{z_{\tau i}}^k \quad \text{with} \quad \tau = 1,\dots,M_{u_z} \quad \text{and} \quad i = 1,\dots,N_n \end{aligned} \tag{9}$$

Please note the upperscript i for each expansion function F. For the continuation of the explanation, it is convenient to define a compact notation for the real and the virtual systems as shown below:

$$u_l^k = N_i F_{u_l\tau}^{ki} q_{l_{\tau i}}^k = \sum_{i=1}^{N_n} \sum_{\tau=1}^{M_{u_l}} N_i F_{u_l\tau}^{ki} q_{l_{\tau i}}^k \tag{10}$$

$$\delta u_m^k = N_j F_{u_m s}^{kj} \delta q_{m_{sj}}^k = \sum_{j=1}^{N_n} \sum_{s=1}^{M_{u_m}} N_j F_{u_m s}^{kj} \delta q_{m_{sj}}^k \tag{11}$$

where l and m can take the values x, y and z. The summations over i (or j) and τ (or s) have been explicitly written in the previous formulae for the sake of clarity. Furthermore, it is clear that there is no summation over l (or m). This formulation will be useful for the assembly of the matrices of the linear structural system, explained in the following Sec. 4.

4 Governing equations and Finite Element matrices

In this section, the governing equations are derived by using the novel methodology.

4.1 Derivation

In classical elasticity, the stress tensor, $\boldsymbol{\sigma}^k$, and strain tensor, $\boldsymbol{\epsilon}^k$, are conveniently represented in the following vector form:

$$\boldsymbol{\sigma} = \left\{ \begin{array}{cccccc} \sigma_{xx}^k & \sigma_{yy}^k & \sigma_{zz}^k & \sigma_{yz}^k & \sigma_{xz}^k & \sigma_{xy}^k \end{array} \right\}^T, \quad \boldsymbol{\epsilon}^k = \left\{ \begin{array}{cccccc} \epsilon_{xx}^k & \epsilon_{yy}^k & \epsilon_{zz}^k & \epsilon_{yz}^k & \epsilon_{xz} & \epsilon_{xy}^k \end{array} \right\}^T \tag{12}$$

The geometric relationships between strains and displacements can be defined as:

$$\boldsymbol{\epsilon}^k = \mathbf{D}\mathbf{u}^k \tag{13}$$

where $\mathbf{D}$ represents the matrix of differential operators, applicable in the case of small displacements and angles of rotation:

$$\mathbf{D} = \begin{bmatrix} \partial_x & 0 & 0 \\ 0 & \partial_y & 0 \\ 0 & 0 & \partial_z \\ 0 & \partial_z & \partial_y \\ \partial_z & 0 & \partial_x \\ \partial_y & \partial_x & 0 \end{bmatrix} \tag{14}$$

In this study, linear elastic orthotropic materials are considered, leading to the following constitutive relation:

$$\boldsymbol{\sigma}^k = \mathbf{C}^k \boldsymbol{\epsilon}^k \tag{15}$$

where $\mathbf{C}^k$ is the matrix of the material coefficients and it can be found in [4].
To derive the governing equations for the novel beam FEs, the principle of virtual work is employed, which states:

$$\delta L_{int} = \delta L_{ext} \tag{16}$$

First, the internal work must be taken into account, and its explicit expression is given as follows:

$$\delta L_{int} = \int_V \delta \boldsymbol{\epsilon}^{kT} \boldsymbol{\sigma}^k \mathrm{d}V = \int_V \left(\delta\epsilon_{xx}^k \sigma_{xx}^k + \delta\epsilon_{yy}^k \sigma_{yy}^k + \delta\epsilon_{zz}^k \sigma_{zz}^k + \delta\epsilon_{yz}^k \sigma_{yz}^k + \delta\epsilon_{xz}^k \sigma_{xz}^k + \delta\epsilon_{xy}^k \sigma_{xy}^k \right) \mathrm{d}V^k \tag{17}$$

where $\mathrm{d}V = \mathrm{d}x\mathrm{d}y\mathrm{d}z$. Using displacement-strain relation (Eq. (13)), the CUF and the FEM approximations (Eq. (10)), and the constitutive equations (Eq. (15)), it is possible to arrive to the following expression for the internal work, which is not given for brevity.
The following expression of the external work may be used for the point loads:

$$\delta L_{ext} = \delta \mathbf{u}^{kT} \mathbf{P}^k = \delta u_x^k P_{u_x}^k + \delta u_y^k P_{u_y}^k + \delta u_z^k P_{u^z}^k \tag{18}$$

By employing the CUF and FEM approximations for the virtual variations (Eq. (10)), the following expression can be written:

$$\delta L_{ext} = \delta q_{x_{sj}}^k N_j F_{u_x s}^{kj} P_{u_x}^k + \delta q_{y_{sj}}^k N_j F_{u_y s}^{kj} P_{u_y}^k + \delta q_{z_{sj}}^k N_j F_{u_z s}^{kj} P_{u_z}^k \tag{19}$$

In this way, it is possible to obtain three governing equations for each virtual displacement:

$$\begin{aligned}
\delta q^k_{x_{sj}} &: K^k_{u_x u_x s\tau ji} q^k_{x_{\tau i}} + K^k_{u_x u_y s\tau ji} q^k_{y_{\tau i}} + K^k_{u_x u_z s\tau ji} q^k_{z_{\tau i}} = P^k_{u_x sj} \\
\delta q^k_{y_{sj}} &: K^k_{u_y u_x s\tau ji} q^k_{x_{\tau i}} + K^k_{u_y u_y s\tau ji} q^k_{y_{\tau i}} + K^k_{u_y u_z s\tau ji} q^k_{z_{\tau i}} = P^k_{u_y sj} \\
\delta q^k_{z_{sj}} &: K^k_{u_z u_x s\tau ji} q^k_{x_{\tau i}} + K^k_{u_z u_y s\tau ji} q^k_{y_{\tau i}} + K^k_{u_z u_z s\tau ji} q^k_{z_{\tau i}} = P^k_{u_z sj}
\end{aligned} \tag{20}$$

The fundamental nuclei for the load vector are written in the followings:

$$\begin{aligned}
P^k_{u_x sj} &= N_j F^{kj}_{u_x s} P^k_{u_x} \\
P^k_{u_y sj} &= N_j F^{kj}_{u_y s} P^k_{u_y} \\
P^k_{u_z sj} &= N_j F^{kj}_{u_z s} P^k_{u_z}
\end{aligned} \tag{21}$$

For the sake of completeness, the nine fundamental nuclei of the stiffness matrix are written below:

$$\begin{aligned}
K^k_{u_x u_x s\tau ji} = &\left\langle C^k_{11} N_j N_i F^{kj}_{u_x s,x} F^{ki}_{u_x \tau,x} \right\rangle + \left\langle C^k_{44} N_j N_i F^{kj}_{u_x s,z} F^{ki}_{u_x \tau,z} \right\rangle \\
&+ \left\langle C^k_{16} N_j N_{i,y} F^{kj}_{u_x s,x} F^{ki}_{u_x \tau} \right\rangle + \left\langle C^k_{16} N_{j,y} N_i F^{kj}_{u_x s} F^{ki}_{u_x \tau,x} \right\rangle \\
&+ \left\langle C^k_{66} N_{j,y} N_{i,y} F^{kj}_{u_x s} F^{ki}_{u_x \tau} \right\rangle
\end{aligned} \tag{22}$$

$$\begin{aligned}
K^k_{u_x u_y s\tau ji} = &\left\langle C^k_{12} N_j N_{i,y} F^{kj}_{u_x s,x} F^{ki}_{u_y \tau} \right\rangle + \left\langle C^k_{45} N_j N_i F^{kj}_{u_x s,z} F^{ki}_{u_y \tau,z} \right\rangle \\
&+ \left\langle C^k_{16} N_j N_i F^{kj}_{u_x s,x} F^{ki}_{u_y \tau,x} \right\rangle + \left\langle C^k_{26} N_{j,y} N_{i,y} F^{kj}_{u_x s} F^{ki}_{u_y \tau} \right\rangle \\
&+ \left\langle C^k_{66} N_{j,y} N_i F^{kj}_{u_x s} F^{ki}_{u_y \tau,x} \right\rangle
\end{aligned} \tag{23}$$

$$\begin{aligned}
K^k_{u_x u_z s\tau ji} = &\left\langle C_{13} N_j N_i F^{kj}_{u_x s,x} F^{ki}_{u_z \tau,z} \right\rangle + \left\langle C^k_{44} N_j N_i F^{kj}_{u_x s,z} F^{ki}_{u_z \tau,x} \right\rangle \\
&+ \left\langle C_{45} N_j N_{i,y} F^{kj}_{u_x s,z} F^{ki}_{u_z \tau} \right\rangle + \left\langle C_{36} N_{j,y} N_i F^{kj}_{u_x s} F^{ki}_{u_z \tau,z} \right\rangle
\end{aligned} \tag{24}$$

$$\begin{aligned}
K^k_{u_y u_x s\tau ji} = &\left\langle C^k_{12} N_{j,y} N_i F^{kj}_{u_y s} F^{ki}_{u_x \tau,x} \right\rangle + \left\langle C^k_{45} N_j N_i F^{kj}_{u_y s,x} F^{ki}_{u_x \tau,z} \right\rangle \\
&+ \left\langle C^k_{16} N_j N_i F^{kj}_{u_y s,x} F^{ki}_{u_x \tau,x} \right\rangle + \left\langle C^k_{26} N_{j,y} N_{i,y} F^{kj}_{u_y s} F^{ki}_{u_x \tau} \right\rangle \\
&+ \left\langle C^k_{66} N_j N_{i,y} F^{kj}_{u_y s,x} F^{ki}_{u_x \tau} \right\rangle
\end{aligned} \tag{25}$$

$$\begin{aligned}
K^k_{u_y u_y s\tau ji} = &\left\langle C^k_{22} N_{j,y} N_{i,y} F^{kj}_{u_y s} F^{ki}_{u_y \tau} \right\rangle + \left\langle C^k_{55} N_j N_i F^{kj}_{u_y s,z} F^{ki}_{u_y \tau,z} \right\rangle \\
&+ \left\langle C^k_{26} N_j N_{i,y} F^{kj}_{u_y s,x} F^{ki}_{u_y \tau} \right\rangle + \left\langle C^k_{26} N_{j,y} N_i F^{kj}_{u_y s} F^{ki}_{u_y \tau,x} \right\rangle \\
&+ \left\langle C^k_{66} N_j N_i F^{kj}_{u_y s,x} F^{ki}_{u_y \tau,x} \right\rangle
\end{aligned} \tag{26}$$

$$\begin{aligned}
K^k_{u_y u_z s\tau ji} = &\left\langle C^k_{23} N_{j,y} N_i F^{kj}_{u_y s} F^{ki}_{u_z \tau,z} \right\rangle + \left\langle C^k_{55} N_j N_{i,y} F^{kj}_{u_y s,z} F^{ki}_{u_z \tau} \right\rangle \\
&+ \left\langle C^k_{45} N_j N_i F^{kj}_{u_y s,z} F^{ki}_{u_z \tau,x} \right\rangle + \left\langle C^k_{45} N_j N_i F^{kj}_{u_y s,x} F^{ki}_{u_z \tau,z} \right\rangle
\end{aligned} \tag{27}$$

$$K^k_{u_z u_x s\tau ji} = \left\langle C^k_{13} N_j N_i F^{kj}_{u_z s,z} F^{ki}_{u_x \tau,x} \right\rangle + \left\langle C^k_{44} N_j N_i F^{kj}_{u_z s,x} F^{ki}_{u_x \tau,z} \right\rangle + \left\langle C^k_{45} N_{j,y} N_i F^{kj}_{u_z s} F^{ki}_{u_x \tau,z} \right\rangle + \left\langle C^k_{36} N_j N_{i,y} F^{kj}_{u_z s,z} F^{ki}_{u_x \tau} \right\rangle \tag{28}$$

$$K^k_{u_z u_y s\tau ji} = \left\langle C^k_{23} N_j N_{i,y} F^{kj}_{u_z s,z} F^{ki}_{u_y \tau} \right\rangle + \left\langle C^k_{55} N_{j,y} N_i F^{kj}_{u_z s} F^{ki}_{u_y \tau,z} \right\rangle + \left\langle C^k_{45} N_j N_i F^{kj}_{u_z s,x} F^{ki}_{u_y \tau,z} \right\rangle + \left\langle C^k_{36} N_j N_i F^{kj}_{u_z s,z} F^{ki}_{u_y \tau,x} \right\rangle \tag{29}$$

$$K^k_{u_z u_z s\tau ji} = \left\langle C^k_{33} N_j N_i F^{kj}_{u_z s,z} F^{ki}_{u_z \tau,z} \right\rangle + \left\langle C^k_{55} N_{j,y} N_{i,y} F^{kj}_{u_z s} F^{ki}_{u_z \tau} \right\rangle + \left\langle C^k_{45} N_j N_{i,y} F^{kj}_{u_z s,x} F^{ki}_{u_z \tau} \right\rangle + \left\langle C^k_{45} N_{j,y} N_i F^{kj}_{u_z s} F^{ki}_{u_z \tau,x} \right\rangle + \left\langle C^k_{44} N_j N_i F^{kj}_{u_z s,x} F^{ki}_{u_z \tau,x} \right\rangle \tag{30}$$

where $\langle(\cdots)\rangle = \int_V (\cdots)\,\mathrm{d}V$.

4.2 Assembly

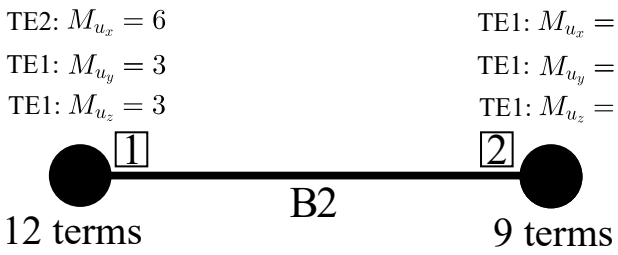

Figure 6: Example of a beam element. For each node, a different theory is adopted. While the second node uses only first-order expansions, the first node adopts a second-order expansion for u_x.

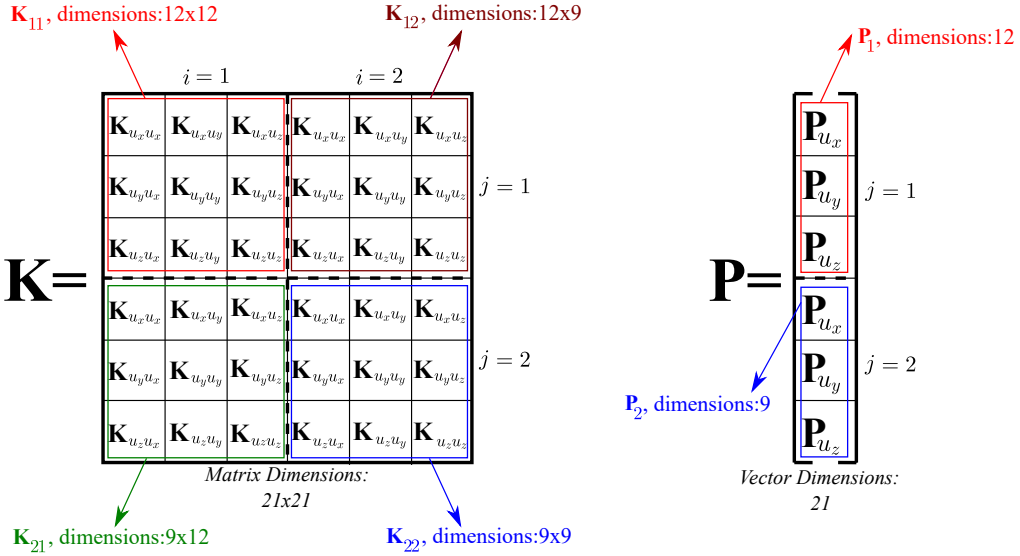

Figure 7: Assembly of the structural stiffness matrix and load vector.

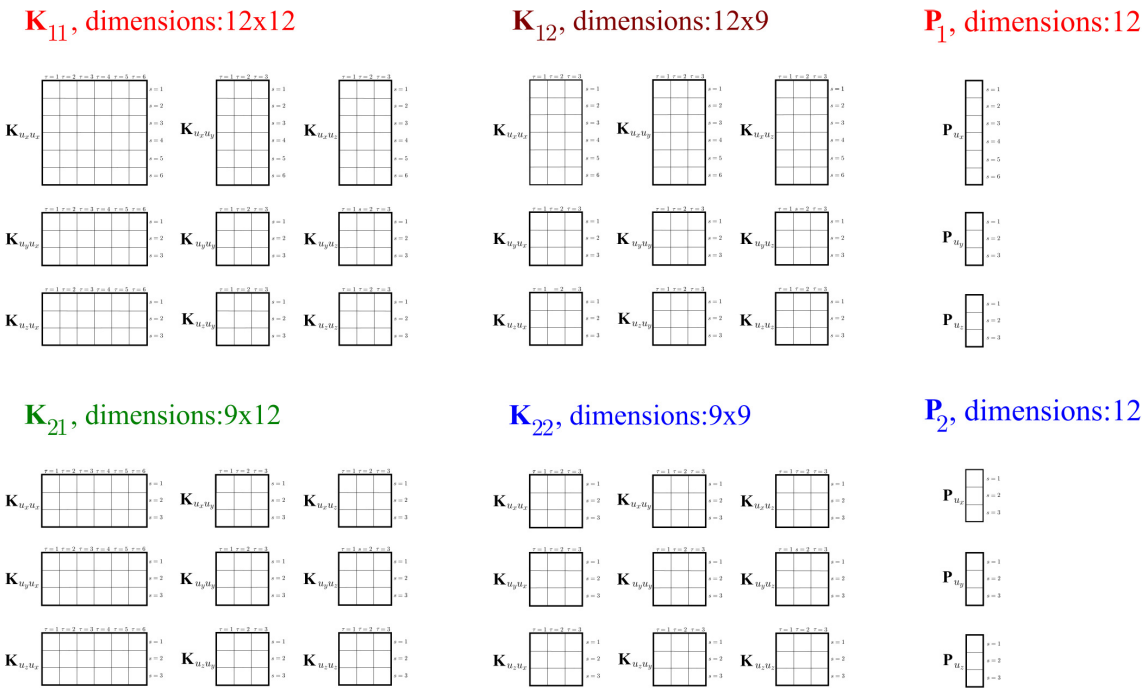

Figure 8: Detailed illustration of the stiffness matrix and the load vector.

In this section, a simple example helps to understand the assembling process of the FE matrices in the context of Unified Formulation connected to the NDK method. Figure 6 shows a simple two-node beam element (B2). In the first node, u_x is studied by a second-order Taylor model (TE2), while u_y and u_z adopt a first-order model (TE1). The second FE node adopts TE1 for each displacement variable. Practically, the first node has 12 terms, while the other owns 9 terms. The total number of degrees of freedom for the entire structure is 21.

In Fig. 7, the stiffness matrix with dimensions of 21×21 and the load vector with dimensions of 21 are illustrated for the entire structure. Each sub-matrix $\mathbf{K}_{ji}$ and sub-vector $\mathbf{P}_j$ have different dimensions since each FE node possesses a different number of terms. Furthermore, Fig. 8 shows how the sub-matrices $\mathbf{K}_{ji}$ and the sub-vectors $\mathbf{P}_j$ are subdivided into nine and three sub-arrays, respectively. Then, each sub-array is composed of a different number of scalar fundamental nuclei (FN), which depend on the number of terms of each FE node and displacement variable. Thus, every $\mathbf{K}_{u_m u_l ji}$ (or $\mathbf{P}_{u_m j}$) has different dimensions and shapes.

5 Numerical Results and Discussion

In the present section, three examples are considered in an extended way, focusing on both displacements and stresses. The first one deals with the end-effects on a beam structure near the clamped section. In the second benchmark, a thin-walled beam with a C-shaped cross-section is taken into account. The last example has the same geometric properties as the second structure, but the boundary conditions have been changed.

In these examples, several models are considered: (a) complete Taylor Models; (b) Reduced

Taylor Models; (c) complete Lagrange Models; (d) mixed TE/LE models ; (e) NDK models. For the latter, figures are shown to clarify the collocation of different theories along the beam axis. In this way, the NDK models are denoted simply as NDKn. More details are given during the explanation of the benchmarks.

5.1 End-Effects on a clamped beam

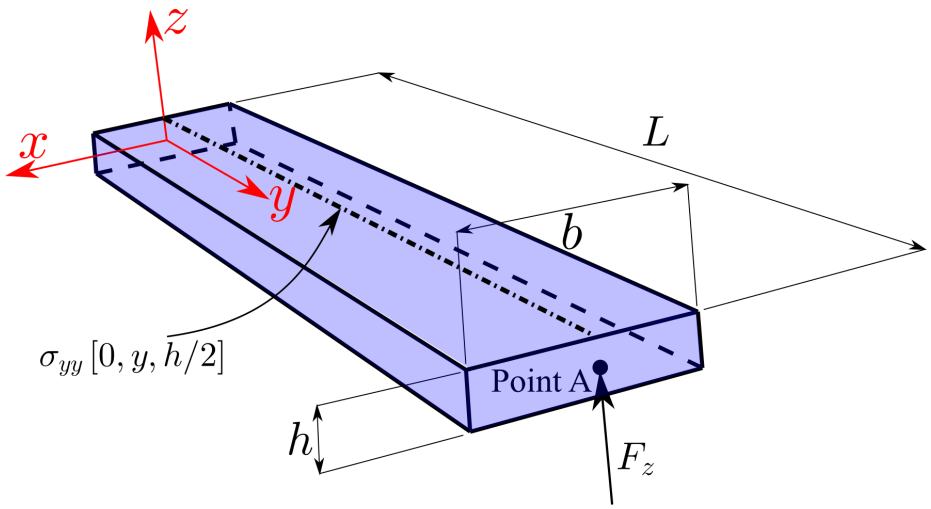

Figure 9: Geometrical properties of a cantilever beam subjected to a point load. The study case is taken from [55].

The first benchmark deals with the end-effects on a cantilevered orthotropic beam, see Fig. 9 for the geometrical properties. The height, h, is equal to 1 [m], and the ratio b/h is 0.5. The aspect ratio, L/h, is equal to six, where L is the length of the structure. The orthotropic material has the following properties: $E_{11} = 206.80$ [GPa], $E_{22} = E_{33} = 5.17$ [GPa], $G_{12} = G_{13} = 3.10$ [GPa], $G_{23} = 2.55$ [GPa], $\nu_{12} = \nu_{23} = \nu_{23} = 0.25$. Concerning the boundary conditions, the beam is clamped at $y = 0$, while a concentrated load is applied in Point A $= [0, L, 0]$ upwards, with a force of magnitude 1 [N]. The results are compared with a higher-order beam theory and a 3D FEM solution illustrated in the paper of Ghazouani and El Fatmi [55]. Also, a complete fifth-order beam theory is used as one of the reference solutions, see Carrera *et al.* [56] for more details. The analysis focuses on the end effects caused by the boundary conditions. Axial stresses, σ_{yy}, are evaluated along $[0, y, h/2]$, as illustrated in Fig. 9. Following the model developed in [56], forty B4 elements are used for all the analyses.

Figure 10 compares the literature solutions. (Please note that the model 1D-TE5 has been derived with the 'classical' CUF method.) The complete uniform present TE5-TE5-TE5 model is chosen as the reference solution for the following analyses.
Since the section of the beam is compact and has a single-layer structure, only Taylor-based models are adopted. Table 1 compares three different types of theories: uniform models, reduced models, and NDK models. The first column is associated with the theory adopted.

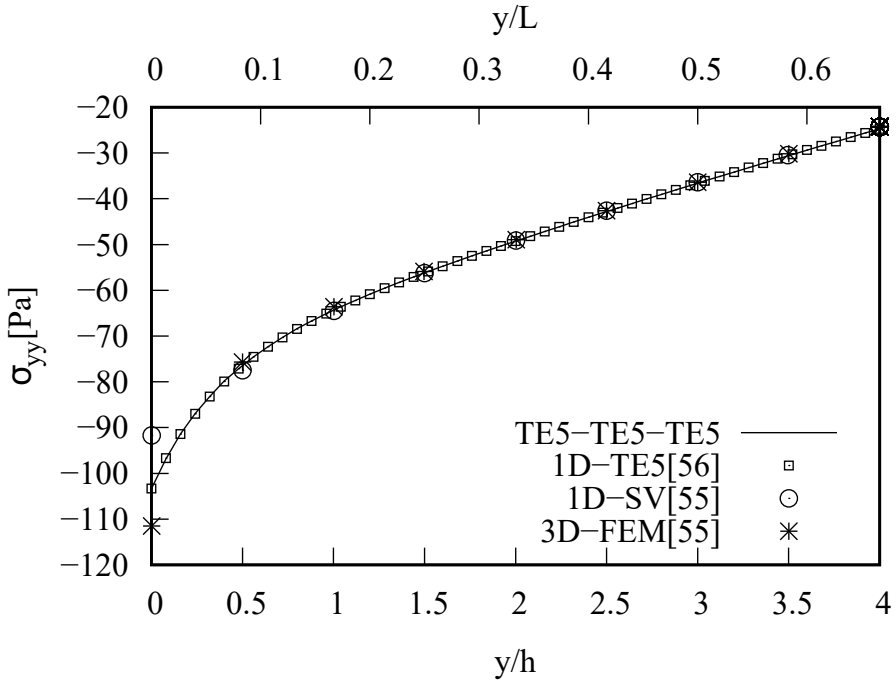

Figure 10: End-effects on a clamped beam for the reference solutions.

Table 1: End effects on a cantilevered plate. The axial stresses are evaluated in $[0, 0, h/2]$.

Model	$-\sigma_{yy}[Pa]$	err [%]	DOF	DOF Reduction [%]
Uniform Models				
TE1	72.000	30.323	1089	85.71
TE2	72.005	30.317	2178	71.43
TE3	93.138	9.8667	3630	52.38
TE4	93.027	9.9741	5445	28.57
TE5[56]	103.33	—[a]	7623	—[a]
Reduced Models				
TE1-TE5-TE5	103.41	0.0758	5445	28.57
TE5-TE1-TE5	72.015	30.308	5445	28.57
TE5-TE5-TE1	102.82	0.5018	5445	28.57
TE1-TE5-TE1	102.67	0.6427	3267	57.14
NDK Models (see Fig. 12)				
NDK 1	103.39	0.0558	4323	43.29
NDK 2	96.138	6.9634	1467	80.76
NDK 3	102.72	0.5945	2167	71.57
NDK 4	102.74	0.5786	2387	68.95
NDK 5	100.57	2.6757	1827	76.03

(a): Taken as the reference solution.

The second and third columns illustrate the axial stresses and the relative error, respectively. The relative error is calculated as follows:

$$\text{err} = \left|\left| \frac{\sigma_{yy}\left(\text{TE5}[56]\right) - \sigma_{yy}}{\sigma_{yy}\left(\text{TE5}[56]\right)} \right|\right| \times 100 \tag{31}$$

The fourth column shows the Degrees Of Freedom (DOF). In the last column, the DOF

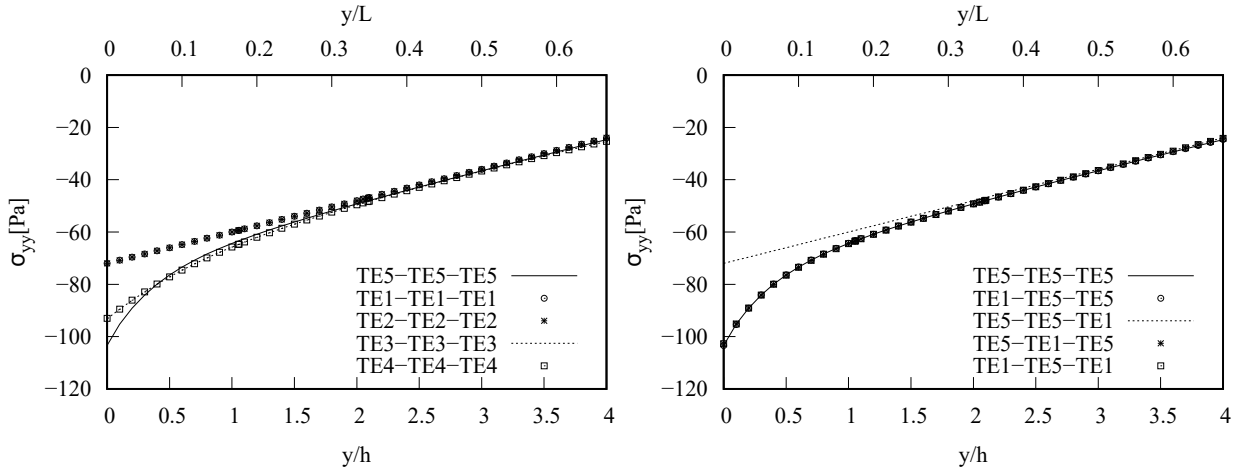

(a) Uniform models (b) Reduced models

Figure 11: End-effects on a cantilevered plate for the present models. The axial stresses, σ_{yy}, are evaluated in $[0, y, h/2]$.

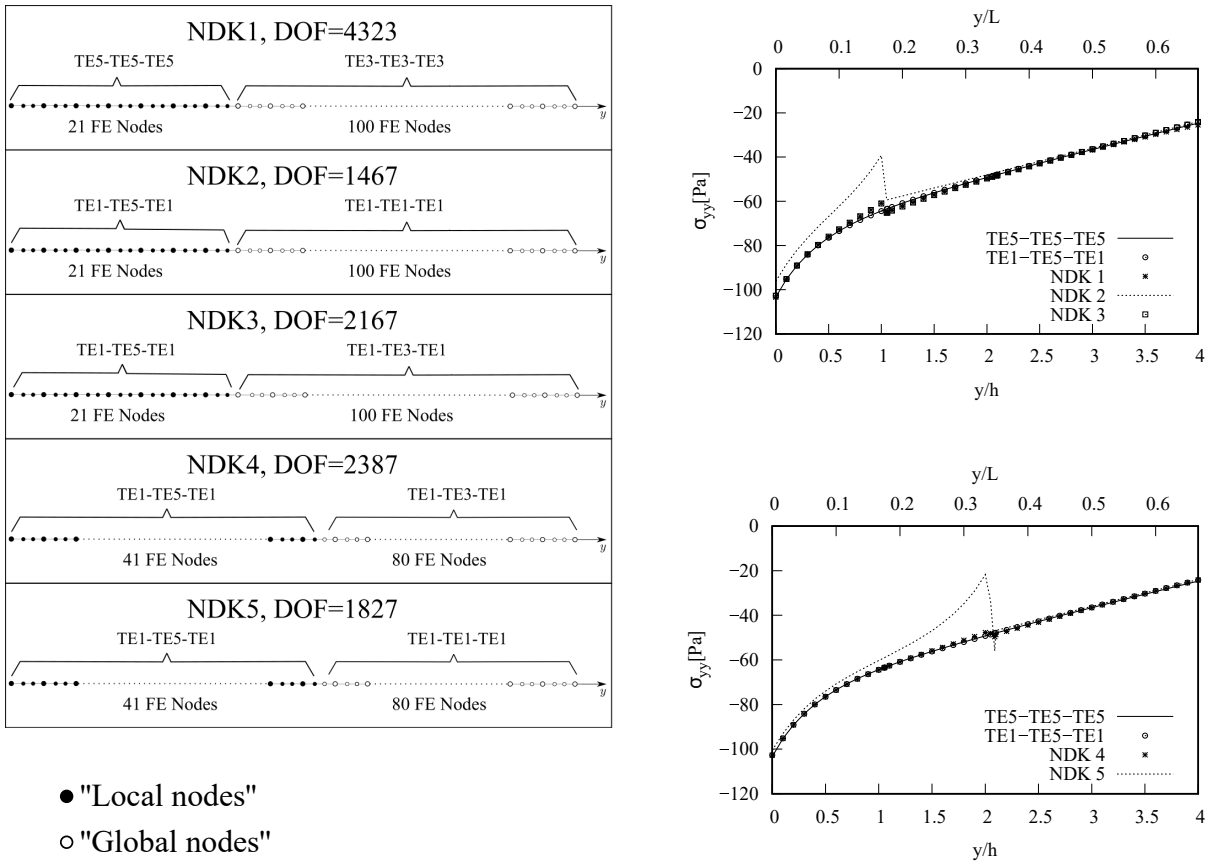

Figure 12: End-effects on a clamped beam for the present NDK solutions. The axial stresses, σ_{yy}, are evaluated in $[0, y, h/2]$.

reduction is shown, which may be found as below:

$$\text{DOF Reduction} = \left|\left| \frac{\text{DOF (TE5[56])} - \text{DOF}}{\text{DOF (TE5[56])}} \right|\right| \times 100 \tag{32}$$

In the first rows, the uniform models from the first to the fifth order are evaluated. Even though a fourth-order model is used, the relative error is about 10 %. From the evaluation of the reduced models, it is possible to understand that a fifth-order model is needed for the displacement variable u_y, while the other two displacement variables are less important to study the axial stresses. The model TE1-TE5-TE1 is very promising since the error is less than 1% and the DOF reduction is about 57%. In the last rows, the NDK models are studied, which are graphically depicted in the left part of Fig. 12. The FE nodes may be divided into two types: (a) 'local nodes', where more refined expansions are used, and (b) 'global nodes,' where less refined models are adopted. NDK1, NDK2, NDK3 adopts twenty-one 'local nodes'. In particular, NDK1 uses only uniform models, while the other two models use also reduced theories to decrease the number of DOFs. On the other hand, NDK4 and NDK5 use a greater number of 'local nodes'.
Figure 11 shows the uniform and the reduced models to understand better how the axial stresses change along the line $[0, y, h/2]$. On the other hand, Fig. 12 shows the trends of axial stresses for the five NDK models.
Other relevant observations can added to the previous ones:

- Notably, the problem exhibits less sensitivity to the model for u_y and u_z. In fact, with the same DOFs, the relative error decreases. Conversely, to attain accurate results, it is essential to retain more terms in models for u_y. However, the importance of the terms changes along the beam axis. In particular, refined expansions are needed near the clamped section;

- Furthermore, some leaps are present when two very different models are used in the 'local' and 'global' parts, as in models NDK2 and NDK5, in the nearby transition element.

5.2 A thin-walled isotropic beam with C-shaped cross-section

The second benchmark is an isotropic thin-walled beam-like structure with a C-shaped cross-section. This analysis was first proposed in Carrera *et al.* [57]. The geometrical properties are shown in Fig. 13. The length, L, is equal to 1 m, the width, a, and the height, h, are 0.1 m, and the thickness, t, is 0.005 m. The structure is clamped at two ends and loaded by a concentrated load $F_z = 1000$ N at Point A $= [a - t, \frac{L}{2}, \frac{h}{2}]$, see Fig. 13b. The used material has the following properties: $E = 71.7$ GPa and $\nu = 0.3$. Concerning the FEM discretization for the present FE models, twenty-two B4 elements are adopted as in [57]. The scheme is depicted in Fig. 14a. The FE mesh is more refined in the area near the load. Lagrange- and Taylor-like expansions are used in the cross-section, see Fig. 14b. As can be seen, the Lagrange expansion over the cross-section allows the refinement of the model in some selected parts of the structure, i.e., near the load. In particular, the complete uniform 12LE9 is adopted in [57], and it is the reference solution for the following analyses.

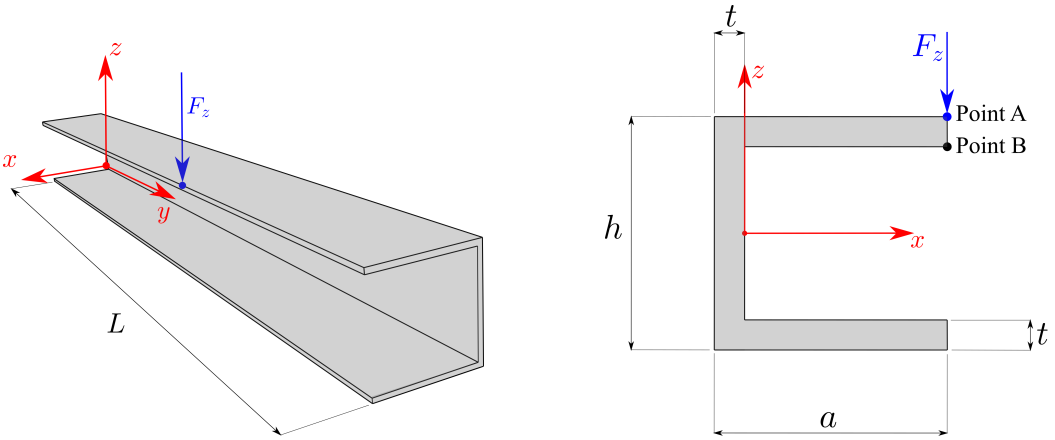

(a) Load (b) Mid-span section

Figure 13: Geometrical properties of the thin-walled isotropic beam with C-shaped cross-section. The study case is taken from [57].

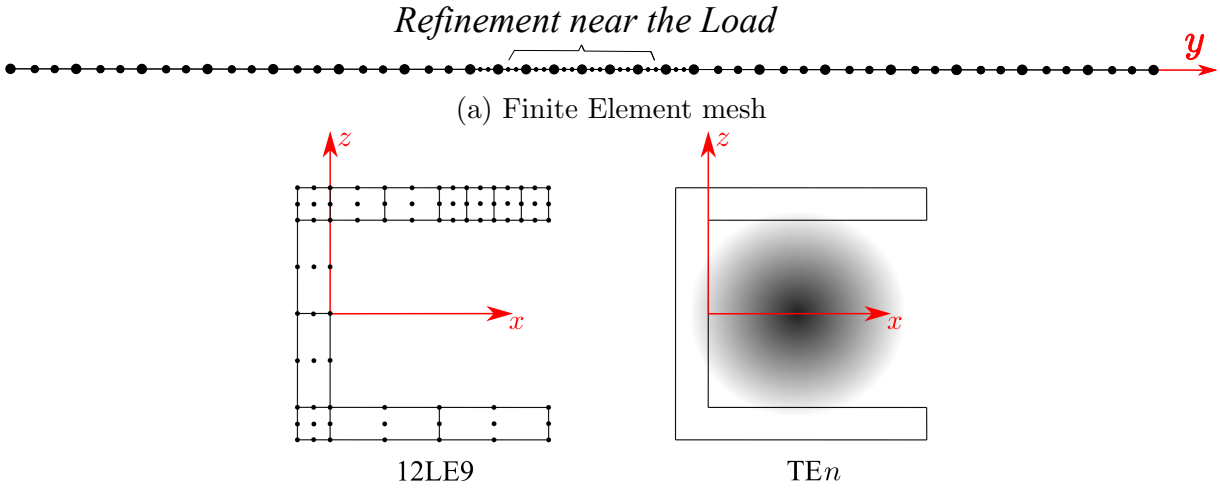

(a) Finite Element mesh

(b) Lagrange and Taylor theories

Figure 14: Thin-walled isotropic beam with C-shaped cross-section. Simplified scheme of the FE mesh (a) and adopted theories (b).

Transverse displacement w is evaluated along the line $[a-t, y, \frac{h}{2}-t]$.

Figure 15 shows four different NDK models. As can be seen, it is possible to model the beam

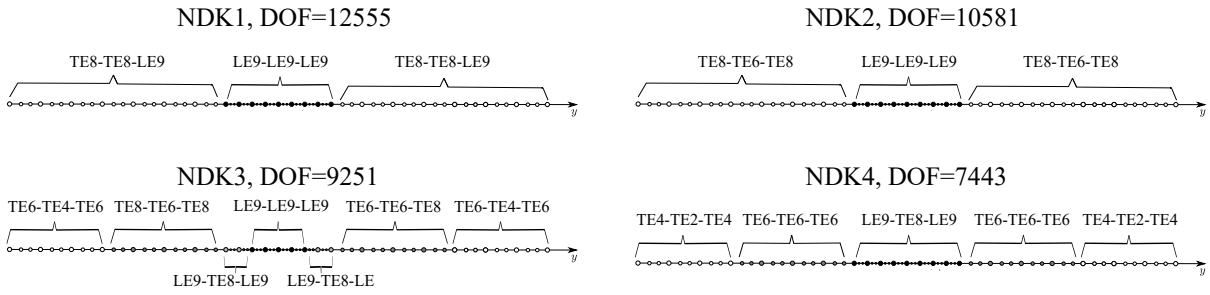

Figure 15: Thin-walled isotropic beam with C-shaped cross-section. Four NDK models.

in a number of ways. In the NDK1 and NDK2 models, the central region uses only uniform

12LE expansions. In the external parts, NDK1 uses a mixed TE-LE expansion TE8-TE8-LE2, while NDK2 uses only Taylor expansion, i.e., TE8-TE6-TE8. In the NDK3, the FE mesh is divided into seven regions, adopting every type of approach. Finally, NDK4 has five regions.

Table 2 shows the transverse displacements in point B $[a-t, L/2, \frac{h}{2}-t]$, displayed in Fig.

Model	w[mm]	err[%]	DOF	DOF Reduction
Uniform models				
LE9[57]	-3.325	—[a]	15075	—[a]
TE4	-0.57033	82.85	3015	80.00
TE8	-2.487	25.20	9045	40.00
TE-LE models				
TE8-LE9-LE9	-2.850	14.29	13065	13.33
LE9-TE8-LE9	-3.170	4.662	13065	13.33
LE9-LE9-TE8	-2.692	19.04	13065	13.33
LE9-TE6-LE9	-2.870	13.68	11926	20.89
NDK models (see Fig. 15)				
NDK1	-3.179	4.391	12555	16.72
NDK2	-2.992	10.02	10581	29.81
NDK3	-2.887	13.18	9251	38.63
NDK4	-2.593	22.02	7443	50.63

(a): Taken as the reference solution.

Table 2: Thin-walled isotropic beam with C-shaped cross-section. Displacements w are calculated in Point B.

13b. In this Table, three different types of theories: uniform models, mixed TE-LE, and NDK models. In general, the Table is structured as the one presented in the previous subsections. The following expression gives the relative error:

$$\text{err} = \left|\left| \frac{\text{w (LE9[57])} - \text{w}}{\text{w (LE9[57])}} \right|\right| \times 100 \tag{33}$$

Instead the DOF reduction respect to the reference solution is calculated through the following relation:

$$\text{DOF Reduction} = \left|\left| \frac{\text{DOF (LE9[57])} - \text{DOF}}{\text{DOF (LE9[57])}} \right|\right| \times 100 \tag{34}$$

In the first rows, the LE9 reference model and two higher-order Taylor-based models are presented. The relative error is above 25%, even though an eight-order model is adopted. Regarding the TE-LE models, the results show that the displacement variable u_y requires less refined expansions over the cross-section. In fact, LE9-TE8-LE9 has a relative error below 5%. It is interesting to see how the model LE9-TE6-LE9 gives better results with respect to TE8-LE9-LE9 and LE9-LE9-TE8, even if having fewer DOFs. The results for the NDK models depicted in Fig. 15 are shown in the last rows. For instance, NDK1 reaches a relatively low error but has higher DOFs. NDK2 is very promising, as the relative error is circa 10% while having a saving of 30% from the computational point of view. Also, the results for NDK3 are quite surprising. On the other hand, NDK4 leads to the worst results.

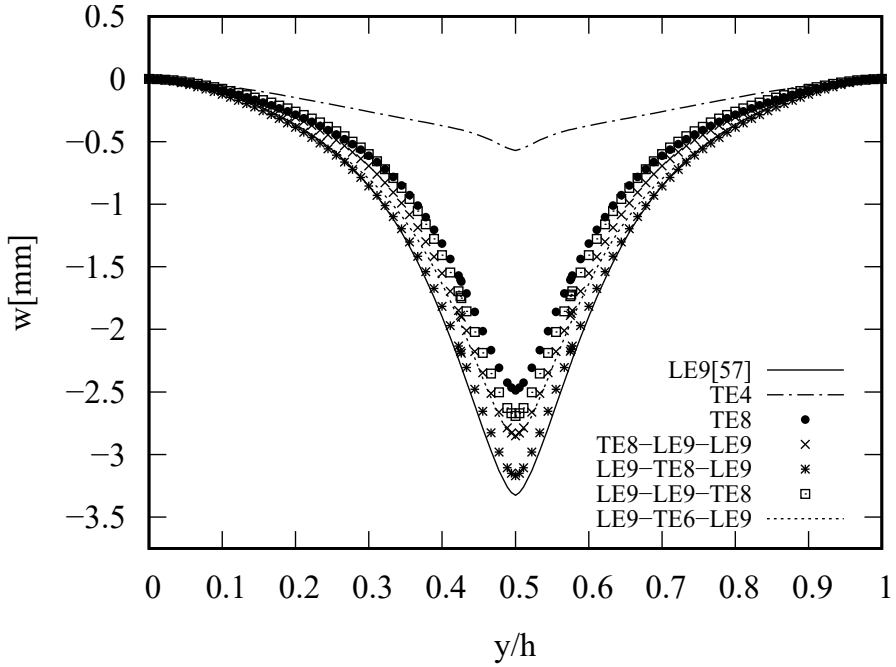

Figure 16: Thin-walled isotropic beam with C-shaped cross-section: variation of w along edge $(a-t, y, h/2-t)$. Uniform and TE-LE models.

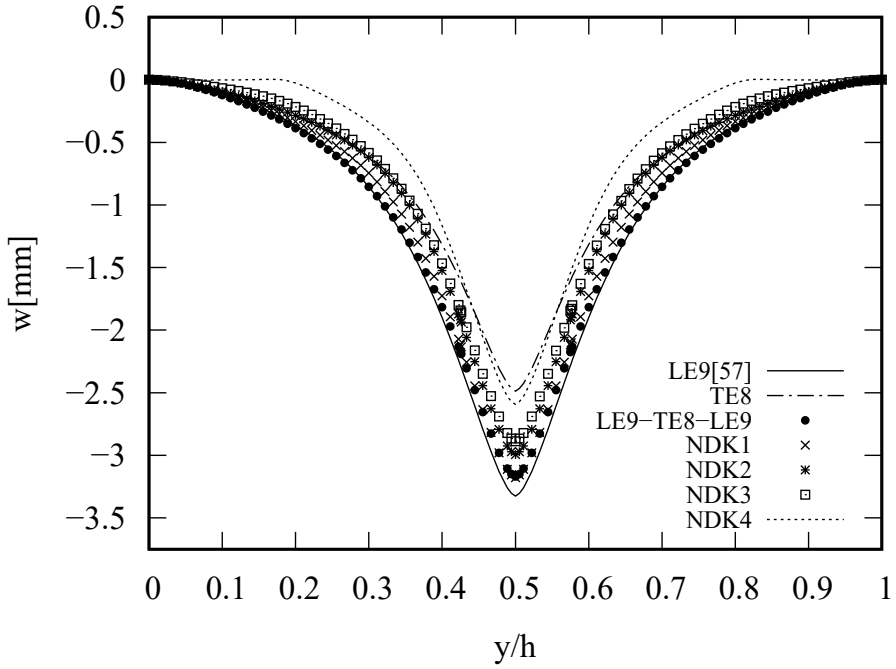

Figure 17: Thin-walled isotropic beam with C-shaped cross-section: variation of w along edge $(a-t, y, h/2-t)$. NDK models.

Figure 16 shows the trend of the transverse displacement along the line $[a-t, y, \frac{h}{2}-t]$ for the uniform models and TE-LE models. On the other hand, Fig. 16 illustrates the results for the NDK models. At last, Fig. 18 compares the contour plots of four different models: LE9, TE8, LE9-TE8-LE9, and NDK3.
The following considerations can be drawn:

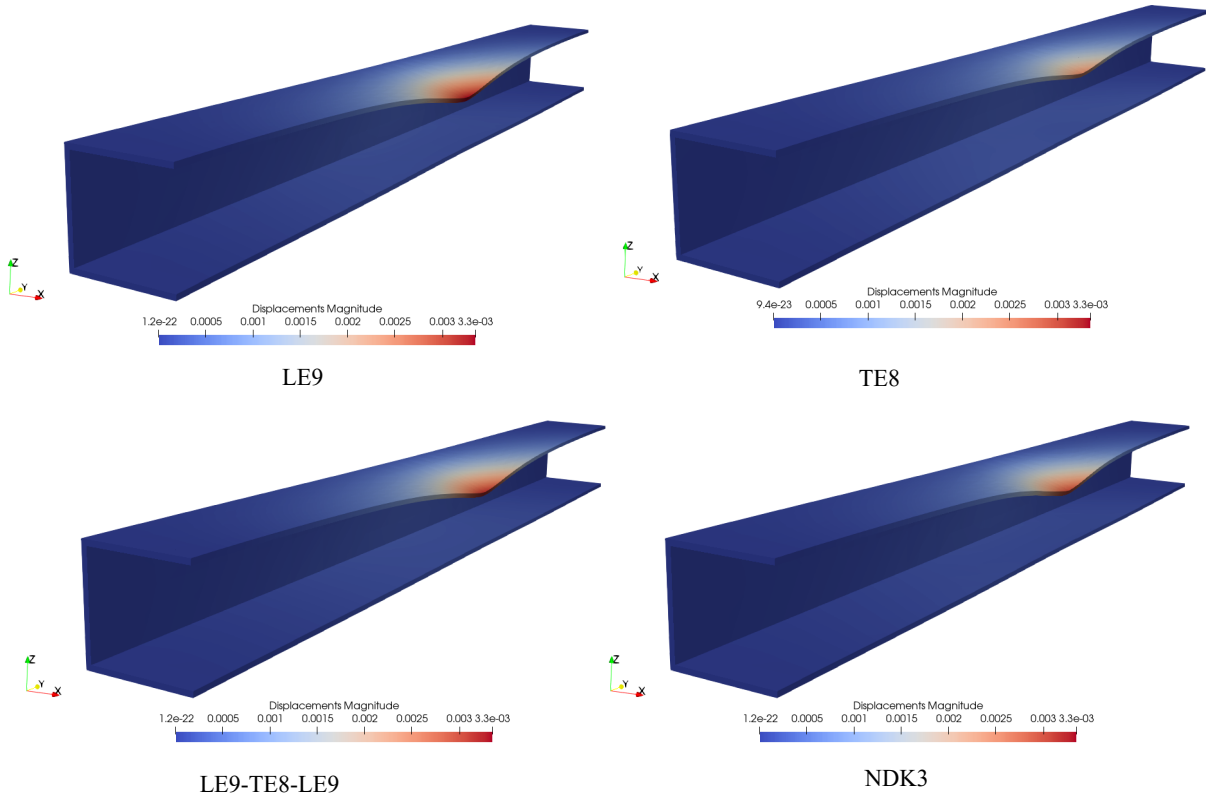

Figure 18: Thin-walled isotropic beam with C-shaped cross-section: contour plot.

- The graphs and the contour plot clearly show how the effect of the loading is limited to the upper central part of the structure. In this way, it is more convenient to use Lagrange expansions and very refined Taylor expansions in the loaded area;
- It is useful to introduce several regions with the use of different expansions;
- The preliminary results for the uniform and mixed TE-LE models have permitted to understand that the displacement variable u_y is less critical for the calculation the solution.

5.3 A thin-walled isotropic beam with C-shaped cross-section loaded by pinching forces

The last example deals with the same structure presented in the previous subsection. Also, the material used is the same. However, the geometrical boundary conditions and the loadings have been changed, as illustrated in Fig. 19. The structure is clamped at the mid-section. The forces at $y = 0$ tend to open the section, while the other pair of forces close the section at the tip. They are located at Point A $= [a - t, 0, \frac{h}{2}]$, Point B $= [a - t, 0, -\frac{h}{2}]$, Point C $= [a - t, L, \frac{h}{2}]$, and Point D $= [a - t, L, -\frac{h}{2}]$. Each force F_z has a module equal to 1000 [N]. Fig. 20a illustrates the FE mesh for this example. Now, a uniform mesh of eighteen four-node Lagrange elements is adopted along the y-axis. Thus, the total of the FE nodes is equal to fifty-five. The expansion for the reference solution is described in Fig. 20b. Sixteen

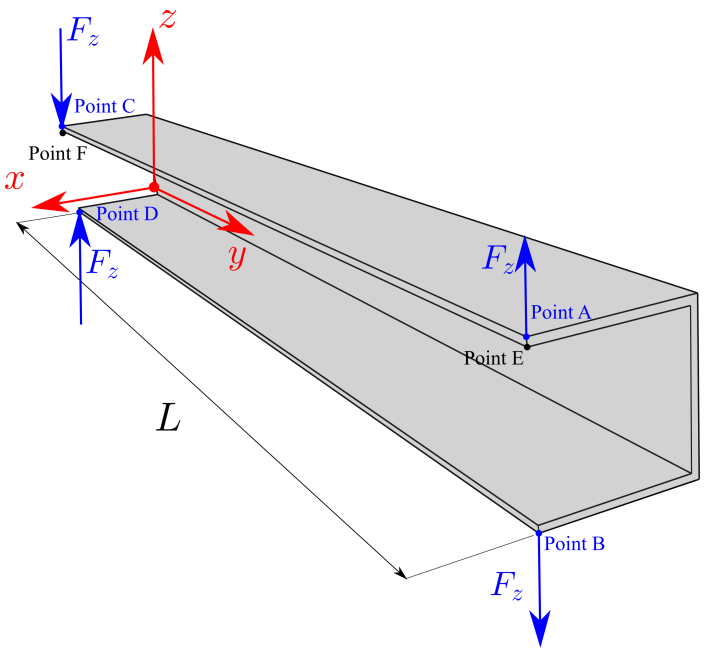

Figure 19: Geometrical properties of the thin-walled isotropic beam with C-shaped cross-section loaded by pinching forces.

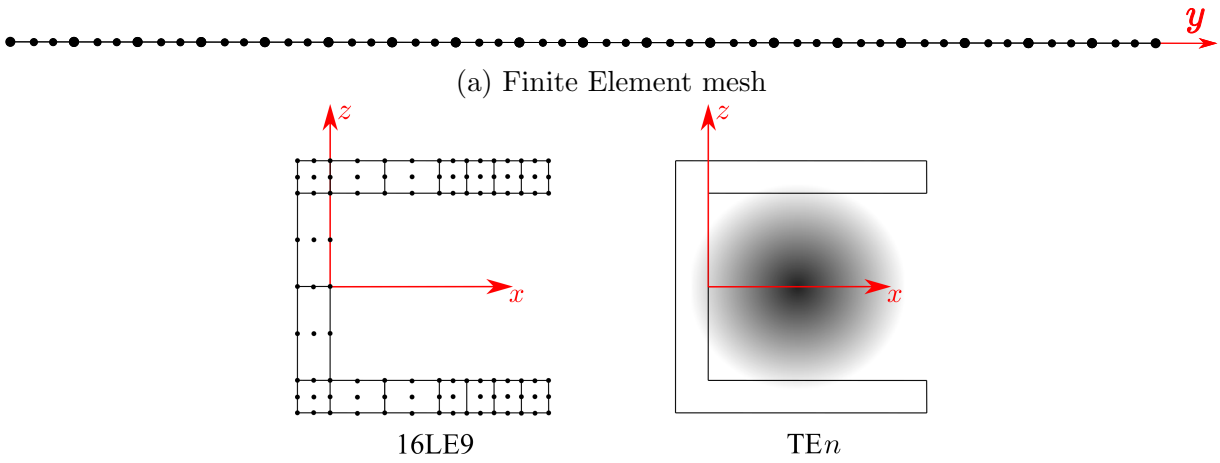

(a) Finite Element mesh

(b) Lagrange and Taylor theories

Figure 20: Thin-walled isotropic beam with C-shaped cross-section loaded by pinching forces. Simplified scheme of the FE mesh (a) and adopted theories (b).

Lagrange-based elements are used over the cross-section. The goal of this subsection is to provide results for a new benchmark. Transverse displacement w are evaluated in Point E $[a-t, 0, \frac{h}{2}-t]$ and Point F $[a-t, L, \frac{h}{2}-t]$.

Figure 21 illustrates the NDK models used in the following analyses. In the NDK1 model, the initial and last nodes adopt a uniform LE9-LE9-LE9, while the inner part uses TE4-TE4-TE6. For the NDK2 model, the outer nodes use a mixed TE8-TE8-LE9 expansion. NDK3 model is similar to the first one, but a less refined expansion, i.e., TE2-TE2-TE4, is adopted in the central nodes. Finally, the NDK4 model inserts TE4-TE4-TE6 in some nodes near the most refined expansion.

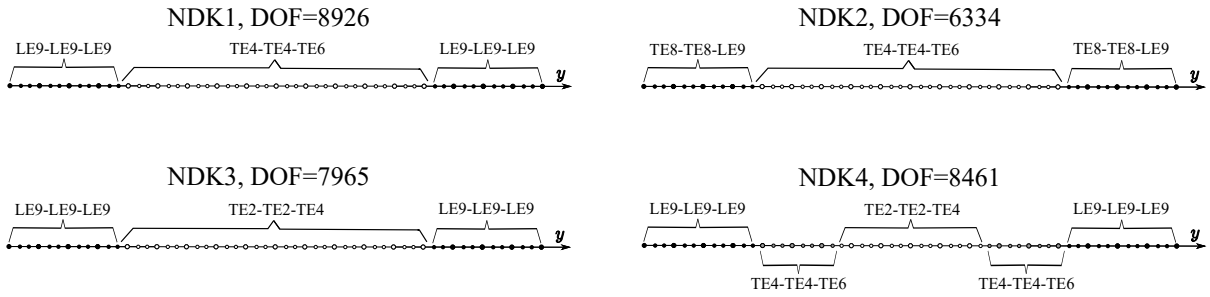

Figure 21: Thin-walled isotropic beam with C-shaped cross-section loaded by pinching forces. Four NDK models.

Table 3 shows the transverse displacements evaluated at Points E and F. As in the previous

Model	w[mm] @ Point E	err[%]	w[mm] @ Point F	err[%]	DOF	DOF Reduction
Uniform models						
LE9	7.987	—[a]	-7.956	—[a]	16335	—[a]
TE2	0.010	99.88	-0.010	99.87	990	93.93
TE4	0.449	94.38	-0.443	94.43	2475	84.84
TE6	4.097	48.71	-4.077	48.78	4620	71.71
TE8	5.706	28.56	-5.682	28.60	7425	54.55
TE10	6.679	16.38	-6.653	16.41	10890	33.33
TE-LE models						
TE4-LE9-LE9	5.326	33.32	-5.326	33.39	11715	28.28
LE9-TE4-LE9	5.185	35.08	-5.185	35.10	11715	28.28
LE9-LE9-TE4	0.694	91.32	-0.685	91.39	11715	28.28
TE4-TE4-LE9	2.914	63.51	-2.914	63.56	7095	56.57
TE8-LE9-LE9	7.060	11.61	-7.033	11.64	13365	18.18
LE9-TE8-LE9	7.313	8.447	-7.287	8.447	13365	18.18
LE9-LE9-TE8	5.791	27.50	-5.766	27.55	13365	18.18
TE8-TE8-LE9	6.347	20.54	-6.322	20.56	10395	36.37
NDK models (see Fig. 21)						
NDK1	7.783	2.620	-7.755	2.636	8926	45.37
NDK2	6.166	29.55	-6.141	29.49	6334	61.22
NDK3	7.540	5.933	-7.541	5.969	7965	51.24
NDK4	7.770	2.796	-7.741	2.813	8461	48.20

(a): Taken as the reference solution.

Table 3: Thin-walled isotropic beam with C-shaped cross-section loaded by pinching forces. Displacements w are calculated in Points E and F, see Fig. 19.

examples, uniform models, mixed TE-LE, and NDK models are evaluated. Also, the formal structure of the Table is based on the previous ones. The relative error and the DOF reduction are calculated with the following formulae:

$$\text{err} = \left|\left| \frac{\text{w}\,(\text{LE9}) - \text{w}}{\text{w}\,(\text{LE9})} \right|\right| \times 100 \tag{35}$$

$$\text{DOF Reduction} = \left|\left|\frac{\text{DOF (LE9)} - \text{DOF}}{\text{DOF (LE9)}}\right|\right| \times 100 \tag{36}$$

For the uniform models, the LE9 is taken as the reference expansion. Also, very higher-order Taylor-based expansions are not sufficient to be close to the best results. In the central part of the Table, the analyses of the mixed TE-LE models are shown. However, the models are kept equal for all the FE nodes. From these results, it is apparent that the displacement variable u_z is the most important one. Coherently, the best model is the LE9-TE8-LE9 for both points, even though the DOF reduction is only about 18 %. TE8-TE8-LE9 is the second-best model in this family of theories. Instead, the last four rows show the NDK analyses presented in Fig. 21. It is possible to consistently lower the total DOFs while maintaining very good results for both evaluated points. It is worth noting that the complete LE9 expansion is needed for the nodes near the loading conditions.

At last, the contour plots of four different models, i.e., LE9, TE8, LE9-TE8-LE9, and NDK3,

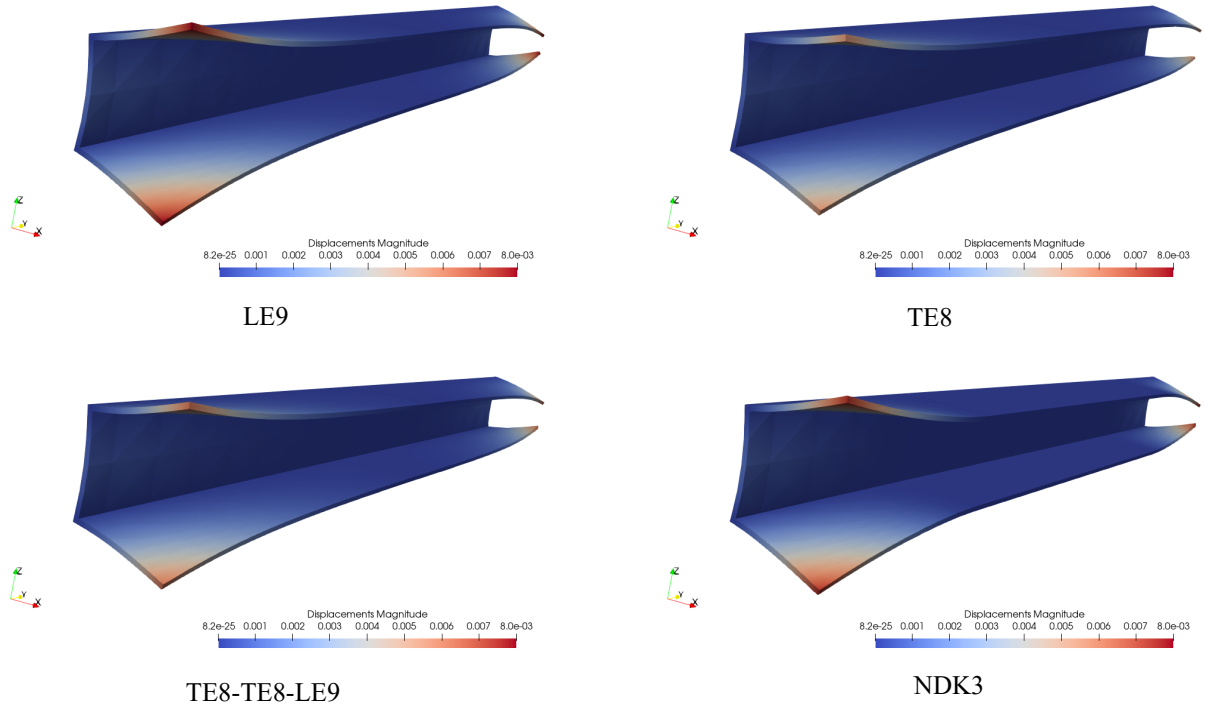

Figure 22: Thin-walled isotropic beam with C-shaped cross-section loaded by pinching forces. Contour plots.

are compared in Fig. 22. The latter has been chosen because of both relatively low error and DOFs with respect to the LE9 reference solution.

The following considerations can be drawn:

- The results demonstrate the importance of using the Lagrange expansions near the two loaded cross-sections. However, the sections around the mid-span of the beam may be studied by less-refined Taylor expansions;
- Also, in this case, it is possible to use several regions with different expansions as in the model NDK4;

- For this very case, the relevance of the displacement variable u_z is much more important than the other two.

6 Conclusions

The present work introduced an improved method to study beam structures based on the Carrera Unified Formulation. Such a method has been obtained by reformulating the previous CUF approach and reordering the way to assemble the Finite Element (FE) matrices. The work is based on two features: (1) it is possible to adopt different expansions for each displacement variable. In particular, Taylor- and Lagrange-based expansions are employed. (2) The Node-Dependent Kinematics (NDK) approach has been introduced. The latter permits the adoption of a different model for each FE node.
To validate the presented formulation, three cases have been studied, ranging from compact to thin-walled structures with isotropic and orthotropic materials. Different types of loadings and boundary conditions were also used. The results have been compared with those taken from the open literature when available. The principal results of the paper may be summarized in the following:

- The method has been demonstrated to be effective in joining different kinds of expansions and polynomial orders;
- It is possible to greatly reduce the degrees of freedom by accurately choosing the expansions for each FE node;
- It is useful to apply local kinematic refinements while keeping the same FE mesh;
- No additional coupling or superposition methods must be applied to the FE matrices;
- The determination of the most efficient models is highly dependent on the nature of the problem taken into account. Please refer to Benchmarks 2 and 3.

Next work could be directed to extend this method to the plate and shell formulations and the multifield and nonlinear analyses.

References

[1] E. Carrera and E. Zappino. One-dimensional finite element formulation with node-dependent kinematics. *Computers & Structures*, 192:114–125, 2017.

[2] L. Euler. *Methodus inveniendi lineas curvas maximi minimive proprietate gaudentes sive solutio problematis isoperimetrici latissimo sensu accepti*, volume 1. Springer Science & Business Media, Berlin, Germany, 1952.

[3] S.P. Timoshenko. On the transverse vibrations of bars of uniform cross section. *Philosophical Magazine*, 43:125–131, 1922.

[4] K.J. Bathe. *Finite Element Procedure*. Prentice hall, Upper Saddle River, New Jersey, USA, 1996.

[5] J. H. Argyris. Matrix analysis of three-dimensional elastic media - small and large displacements. *AIAA Journal*, 3(1):45–51, 1965.

[6] K.J. Bathe and L.W. Ho. Some results in the analysis of thin shell structures. In W. Wunderlich, E. Stein, and K.J. Bathe, editors, *Nonlinear Finite Element Analysis in Structural Mechanics*, pages 122–150, Berlin, Heidelberg, 1981. Springer Berlin Heidelberg.

[7] V.V. Novozhilov. *Theory of elasticity*. Pergamon, Elmsford, 1961.

[8] R.K. Kapania and S. Raciti. Recent advances in analysis of laminated beams and plates. Part I: Shear effects and buckling. *AIAA journal*, 27(7):923–935, 1989.

[9] R.K. Kapania and S. Raciti. Recent advances in analysis of laminated beams and plates. Part II: Vibrations and wave propagation. *AIAA journal*, 27(7):935–946, 1989.

[10] E. Carrera, A. Pagani, M. Petrolo, and E. Zappino. Recent developments on refined theories for beams with applications. *Mechanical Engineering Reviews*, 2(2):14–00298–14–00298, 2015.

[11] K. Washizu. *Variational Methods in Elasticity and Plasticity*. Pergamon, Oxford, United Kingdom, 1968.

[12] V.Z. Vlasov. *Thin-walled elastic beams*. National Technical Information Service, 1984.

[13] P.O. Friberg. Beam element matrices derived from Vlasov's theory of open thin-walled elastic beams. *International Journal for Numerical Methods in Engineering*, 21(7):1205–1228, 1985.

[14] R.D. Ambrosini, J. D. Riera, and R. F. Danesi. A modified Vlasov theory for dynamic analysis of thin-walled and variable open section beams. *Engineering Structures*, 22(8):890–900, 2000.

[15] I. Mechab, N. El Meiche, and F. Bernard. Analytical study for the development of a new warping function for high order beam theory. *Composites Part B: Engineering*, 119:18–31, 2017.

[16] R. Schardt. Eine Erweiterung der Technischen Biegetheorie zur Berechnung prismatischer Faltwerke. *Der Stahlbau*, 35:161–171, 1966.

[17] M. Ganapathi, B. P. Patel, O. Polit, and M. Touratier. A C^1 finite element including transverse shear and torsion warping for rectangular sandwich beams. *International Journal for Numerical Methods in Engineering*, 45(1):47–75, 1999.

[18] M. Levinson. A new rectangular beam theory. *Journal of Sound and Vibration*, 74(1):81–87, 1981.

[19] T. Kant and B. S. Manjunath. Refined theories for composite and sandwich beams with C° finite elements. *Computers & Structures*, 33:755–764, 2014.

[20] T. Kant and B.S. Manjunatha. Higher-order theories for symmetric and unsymmetric fiber reinforced composite beams with C° finite elements. *Finite Elements in Analysis and Design*, 6(4):303–320, 1990.

[21] B.S. Manjunatha and T. Kant. Different Numerical Techniques for the Estimation of Multiaxial Stresses in Symmetric/Unsymmetric Composite and Sandwich Beams with Refined Theories. *Journal of Reinforced Plastics and Composites*, 12(1):2–37, 1993.

[22] E. Carrera. C° Reissner–Mindlin multilayered plate elements including zig-zag and interlaminar stress continuity. *International Journal for Numerical Methods in Engineering*, 39(11):1797–1820, 1996.

[23] M. Cinefra. Free-vibration analysis of laminated shells via refined MITC9 elements. *Mechanics of Advanced Materials and Structures*, 23(9):937–947, 2016.

[24] E. Carrera and G. Giunta. Refined beam theories based on a unified formulation. *International Journal of Applied Mechanics*, 02(01):117–143, 2010.

[25] E. Carrera, G. Giunta, P. Nali, and M. Petrolo. Refined beam elements with arbitrary cross-section geometries. *Computers & Structures*, 88(5):283–293, 2010.

[26] E. Carrera, G. Giunta, and M. Petrolo. A modern and compact way to formulate classical and advanced beam theories. *Developments in Computational Structures Technology*, pages 75–112, 2010.

[27] E. Carrera and M. Petrolo. Refined beam elements with only displacement variables and plate/shell capabilities. *Meccanica*, 47:537–556, 2012.

[28] A. Pagani, E. Carrera, R. Augello, and D. Scano. Use of lagrange polynomials to build refined theories for laminated beams, plates and shells. *Composite Structures*, 276, 2021.

[29] J. N. Reddy. On computational schemes for global-local stress analysis. *NASA, Langley Research Center, Computational Methods for Structural Mechanics and Dynamics, Part 1*, 1989.

[30] A. K. Noor. Global-local methodologies and their application to nonlinear analysis. *Finite Elements in Analysis and Design*, 2(4):333–346, 1986.

[31] J. Fish, L. Pan, V. Belsky, and S. Gomaa. Unstructured multigrid method for shells. *International Journal for Numerical Methods in Engineering*, 39(7):1181–1197, 1996.

[32] W. Prager. Variational principles for elastic plates with relaxed continuity requirements. *International Journal of Solids and Structures*, 4(9):837–844, 1968.

[33] K. C. Park and C. A. Felippa. A variational principle for the formulation of partitioned structural systems. *International Journal for Numerical Methods in Engineering*, 47(1-3):395–418, 2000.

[34] E. Carrera, A. Pagani, and M. Petrolo. Use of Lagrange multipliers to combine 1D variable kinematic finite elements. *Computers & Structures*, 129:194–206, 2013.

[35] M. A. Aminpour, J. B. Ransom, and S. L. McCleary. A coupled analysis method for structures with independently modelled finite element subdomains. *International Journal for Numerical Methods in Engineering*, 38(21):3695–3718, 1995.

[36] J. B. Ransom. *On multifunctional collaborative methods in engineering science*. National Aeronautics and Space Administration, Langley Research Center, 2001.

[37] F. Brezzi and L. D. Marini. The three-field formulation for elasticity problems. *GAMM-Mitteilungen*, 28(2):124–153, 2005.

[38] P.J. Blanco, R.A. Feijóo, and S.A. Urquiza. A variational approach for coupling kinematically incompatible structural models. *Computer Methods in Applied Mechanics and Engineering*, 197(17):1577–1602, 2008.

[39] P. Blanco, P. Gervasio, and A. Quarteroni. Extended variational formulation for heterogeneous partial differential equations. *Computational Methods in Applied Mathematics*, 11(2):141–172, 2011.

[40] B. H. Dhia. Problèmes mécaniques multi-échelles: la méthode Arlequin. *Comptes Rendus de l'Académie des Sciences - Series IIB - Mechanics-Physics-Astronomy*, 326(12):899–904, 1998.

[41] H. B. Dhia and G. Rateau. The arlequin method as a flexible engineering design tool. *International Journal for Numerical Methods in Engineering*, 62(11):1442–1462, 2005.

[42] F. Biscani, G. Giunta, S. Belouettar, E. Carrera, and H. Hu. Variable kinematic beam elements coupled via Arlequin method. *Composite Structures*, 93(2):697–708, 2011.

[43] T. C. Gmür and R. H. Kauten. Three-dimensional solid-to-beam transition elements for structural dynamics analysis. *International Journal for Numerical Methods in Engineering*, 36(9):1429–1444, 1993.

[44] S. Klarmann, J. Wackerfuß, and S. Klinkel. Coupling 2D continuum and beam elements: a mixed formulation for avoiding spurious stressess. *Computational Mechanics*, 70(6):1145–1166, 2022.

[45] A.R. Hartloper, A. de Castro e Sousa, and D.G. Lignos. Warping-inclusive kinematic coupling in mixed-dimension macro models for steel wide flange beam columns. *Journal of Structural Engineering*, 148(2), 2022.

[46] E. Zappino and E. Carrera. Multidimensional model for the stress analysis of reinforced shell structures. *AIAA Journal*, 56(4):1647–1661, 2018.

[47] M. Filippi I. Kaleel A. Pagani M. Petrolo E. Carrera, A. G. de Miguel and E. Zappino. Global-local plug-in for high-fidelity composite stress analysis in ABAQUS. *Mechanics of Advanced Materials and Structures*, 28(14):1445–1450, 2021.

[48] M. Filippi I. Kaleel A. Pagani M. Petrolo E. Carrera, A. G. de Miguel and E. Zappino. Global-local plug-in for high-fidelity composite stress analysis in Femap/NX Nastran. *Mechanics of Advanced Materials and Structures*, 28(11):1121–1127, 2021.

[49] E. Zappino E. Carrera, D. Scano. One-dimensional Finite Elements with Arbitrary Cross-Sectional Displacement Fields. *Under review*, 2024.

[50] E. Carrera and M. Petrolo. On the Effectiveness of Higher-Order Terms in Refined Beam Theories. *Journal of Applied Mechanics*, 78(2), 2010.

[51] G. Li, A.G. de Miguel, A. Pagani, E. Zappino, and E. Carrera. Finite beam elements based on Legendre polynomial expansions and node-dependent kinematics for the global-local analysis of composite structures. *European Journal of Mechanics - A/Solids*, 74:112–123, 2019.

[52] E. Zappino, D. Scano, and E. Carrera. Finite element models with node-dependent kinematics based on legendre polynomials for the global–local analysis of compact and thin walled beams. *Computer Methods in Applied Mechanics and Engineering*, 415:116212, 2023.

[53] E. Carrera, A. Pagani, and D. Scano. Legendre-based node-dependent kinematics shell models for the global–local analysis of homogeneous and layered structures. *International Journal of Solids and Structures*, 289:112630, 2024.

[54] E. Carrera, M. Cinefra, M. Petrolo, and E. Zappino. *Finite element analysis of structures through unified formulation*. John Wiley & Sons, 2014.

[55] N. Ghazouani and R. El Fatmi. Higher order composite beam theory built on Saint-Venant's solution. Part-II: Built-in effects influence on the behavior of end-loaded cantilever beams. *Composite Structures*, 93(2):567–581, 2011.

[56] E. Carrera, M.Petrolo, and E. Zappino. Performance of CUF approach to analyze the structural behavior of slender bodies. *Journal of Structural Engineering*, 138(2):285–297, 2012.

[57] E. Carrera, E. Zappino, and G. Li. Finite element models with node-dependent kinematics for the analysis of composite beam structures. *Composites Part B: Engineering*, 132:35–48, 2018.